A Peltier cooling system for SiPM temperature stabilization

von

Simon Nieswand

Bachelorarbeit in Physik

vorgelegt der

Fakultät für Mathematik, Informatik und Naturwissenschaften

der Rheinisch-Westfälischen Technischen Hochschule Aachen

Oktober 2012

Erstellt im

III. Physikalischen Institut A

Univ.-Prof. Dr. Thomas Hebbeker

Abstract

Deutsch

Im Rahmen dieser Arbeit wurde die Grundlage eines Temperatur-Stabilisierungs-Systems für Silizium Photomultiplier (SiPMs) entwickelt und getestet. Die grundlegende Idee ist es, einen SiPM sowie einen Sensor, der die Temperatur des SiPMs misst, in die Seite eines kleinen, nach außen thermisch isolierten Kupferblockes einzulassen, an welchen ein Peltier-Element angebracht wird. Um das System zu automatisieren, werden der Temperatursensor und die Stromquelle des Peltier-Elements mit einer Microcontroller-Platine verbunden, auf welcher ein PID-Regler-Algorithmus läuft, um den Stromfluss anzupassen. Zu diesen Zweck wurde eine Peltier-Treiber-Platine entworfen, welche einen Gleichstrom in 16 Schritten zwischen 0 A und ungefähr 5 A einstellen kann und durch den Microcontroller angesteuert wird.
Neben dem Austesten des Arbeitsbereichs des benutzten Aufbaus, wie zum Beispiel erreichbare Temperaturen, Abkühlraten etc., wurden Experimente mit verschiedenen Einstellungen des PID-Regler-Algorithmus durchgeführt, um zu überprüfen, ob und wie eine möglichst genaue Stabilisierung der Temperatur erreicht werden kann. Außerdem wurden Messreihen mit unterschiedlichen Regel-Temperaturen aber gleichen PID-Regler-Parametern durchgeführt, um festzustellen, in welchem Temperaturbereich das Stabilisierungs-System einsetzbar ist.
Es hat sich gezeigt, dass das entwickelte System eine Temperatur-Stabilisierung mit maximalen Abweichungen zwischen gemessener und gewollter Temperatur von $\pm 0.14\,\mathrm{K}$ in einem Bereich zwischen der jeweiligen Umgebungstemperatur und ungefähr 25 K darunter ermöglicht. Die Zeit, die bis zur Stabilisierung vergeht, liegt in der Größenordnung von wenigen Minuten und hängt davon ab, wie tief die Regel-Temperatur unter der Raumtemperatur liegt.

English

In the course of this thesis the basis for an automatic temperature stabilization system for silicon photomultipliers (SiPMs) based on Peltier elements was developed and tested. The basic idea is to embed an SiPM and a monitoring temperature sensor into one side of a small body of copper which is thermally insulated from the outside and attached to a Peltier element. To automate the system, the temperature sensor and the Peltier element's current supply are connected to a

microcontroller board running a PID controller algorithm to adjust the current flow. For this purpose a Peltier driver board was designed to alter direct currents between 0 A and approximately 5 A in 16 steps controlled by the microcontroller. Besides testing the performance of the used setup in terms of achievable temperatures, cooling rates etc., experiments with changes of the controller's parameters were conducted to examine if and how a temperature stabilization can be achieved. Furthermore a series of measurement with different approached temperatures but fixed PID parameters were done to analyze in which region the stabilization system can be used.
It was shown that the developed system can achieve temperature stabilization with maximum deviations of ± 0.14 K between measured and desired temperature over several minutes between the given ambient temperature and roughly 25 K below. The time it takes to stabilize a temperature amounts to a few minutes and depends on how low it lies beneath the room temperature.

Contents

1 Introduction

In modern experimental physics the development of more efficient and more precise detectors for different applications is an ongoing task. A relatively new achievement in low level light detection are silicon photomultipliers (SiPMs) which work on a semiconductor basis and are able to count single photons. Advantages lie in their small size of a few square millimeters and a low operating voltage of approximately 70 V [1]. Furthermore, their signals are not influenced by strong magnetic fields [2].
These properties render them very useful candidates for upgrades of current elementary particle detector systems such as the ones used in the CMS experiment at the Large Hadron Collider in Geneva or the Pierre Auger Observatory in Argentina.
As the Institutes of Physics III A and B of the RWTH Aachen University participate in these experiments, various researches on SiPM characteristics were done over the last years by members of these institutes.
Among other results, the dependence of the current-voltage characteristic of an SiPM on the operating temperature was studied [3]. In figure 1.1 the dark current of an SiPM as a function of the operating voltage is shown for different temperatures.
As can be seen, the dark current proceeds almost constantly for low voltages and rises steeply from a certain voltage on upwards. This voltage is called the breakdown voltage V_b and is the minimum voltage that needs to be applied to an SiPM for it to work. The breakdown voltage is used as a reference for the voltage V_bias at which a SiPM is operated. The gap between these voltages is called the over-voltage and is usually on the order of 1 V.
As shown, V_b increases with higher temperatures T. In figure 1.2 can be seen that the breakdown voltage has a linear dependence on the temperature and changes by about 56 $\frac{\mathrm{mV}}{\mathrm{K}}$ [4]. In relation to typical values of V_b on the order of 70 V this effect might not seem significant for small changes in temperature. But a change in the breakdown voltage also affects the over-voltage

$$V_\mathrm{ov}(T) = V_\mathrm{bias} - V_\mathrm{b}(T) \tag{1.1}$$

and accounts for several percent of it.
The influence of this change can be seen in figure 1.3. The plot shows the deposited charge ΔQ per firing SiPM pixel as function of the operating voltage. This charge is called the gain of an SiPM. The breakdown voltage of about 70 V was determined

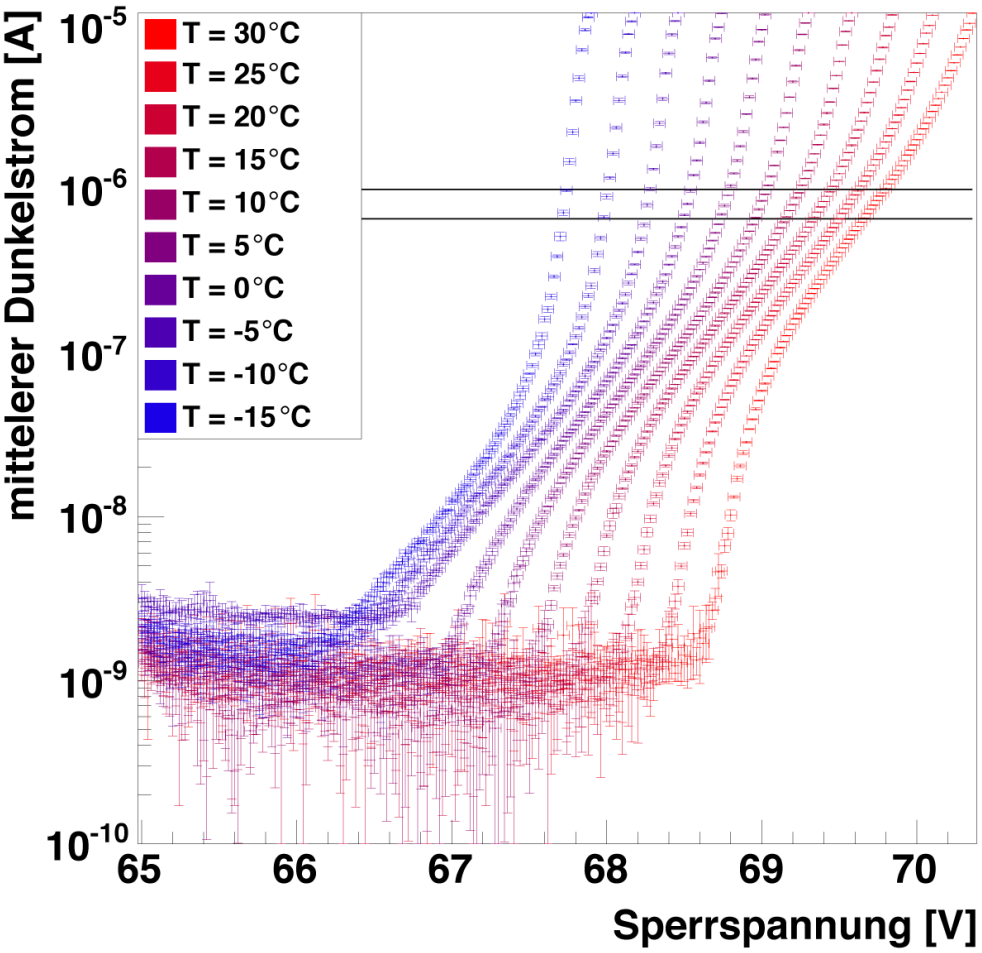

Figure 1.1: Current-voltage characteristic of an SiPM for different temperatures (SiPM-model: Hamamatsu S10362-11-100U). Plot taken from [3].

by extrapolating V_{bias} down to $\Delta Q = 0$. As the breakdown voltage is constant, the plot can also be read as the dependence of the deposited charge on the over-voltage. The change of ΔQ was determined to approx. $12.6\,\frac{\text{pC}}{\text{V}}$. Therefore, the temperature dependence of the gain is given by

$$12.6\,\frac{\text{pC}}{\text{V}} \cdot 56\,\frac{\text{mV}}{\text{K}} = 0.71\,\frac{\text{pC}}{\text{K}} \quad . \tag{1.2}$$

For a typical over-voltage of 1 V and, therefore, an operation voltage of about 71 V the gain is approx. 17 pC. So a change of $0.71\,\frac{\text{pC}}{\text{K}}$ accounts for about $4\,\frac{\%}{\text{K}}$ of the deposited charge. This leads to rather large measurement errors on the number

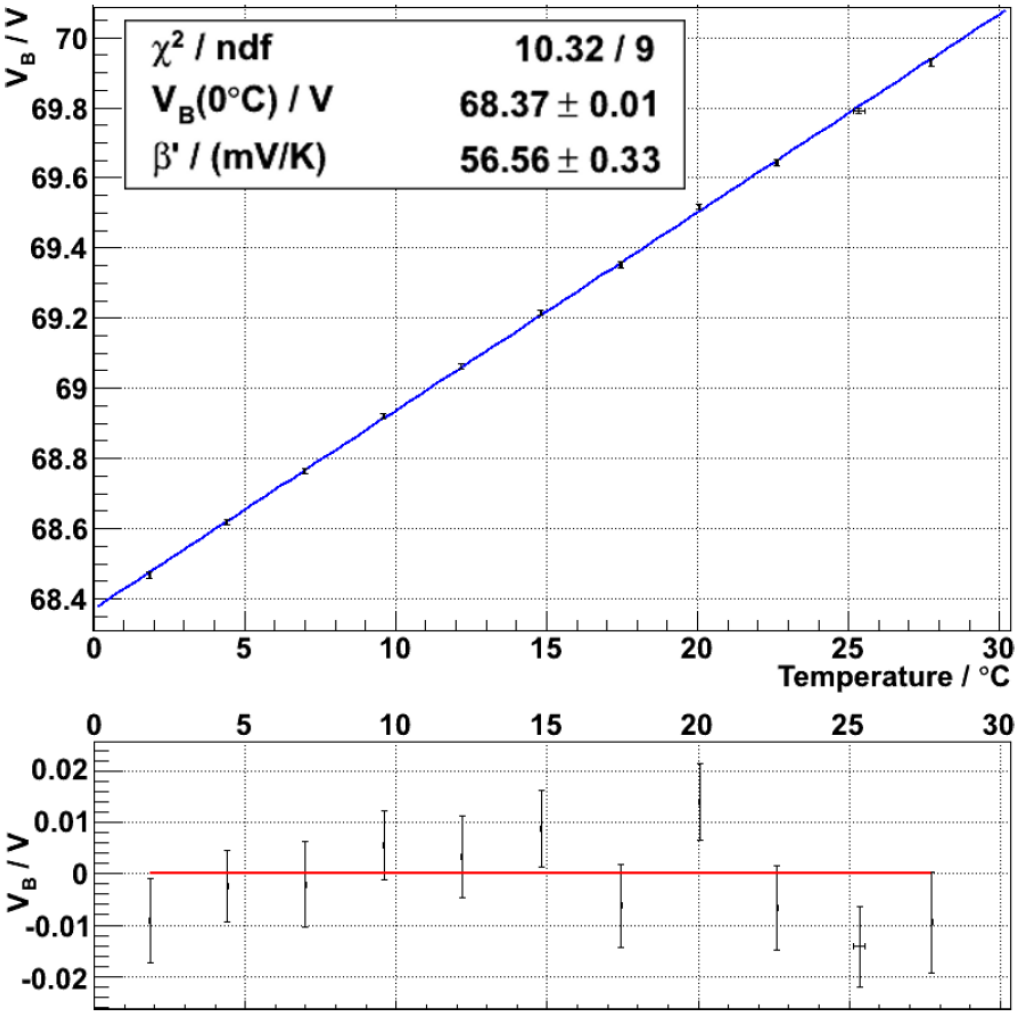

Figure 1.2: Breakdown voltage of an SiPM as a function of the SiPM's temperature (SiPM-model: Hamamatsu S10362-11-100C). Plot taken from [4].

of detected photons for relatively small changes in temperature.
Also, in a case of extreme temperature rises, V_b might exceed the operating voltage leaving the SiPM non-functional.
As can be seen, it is important for several reasons to know the temperature a measurement was taken at and also to maintain a stable temperature for the period of an experiment.
Besides that, it is also beneficial to cool down the SiPM, because as shown in

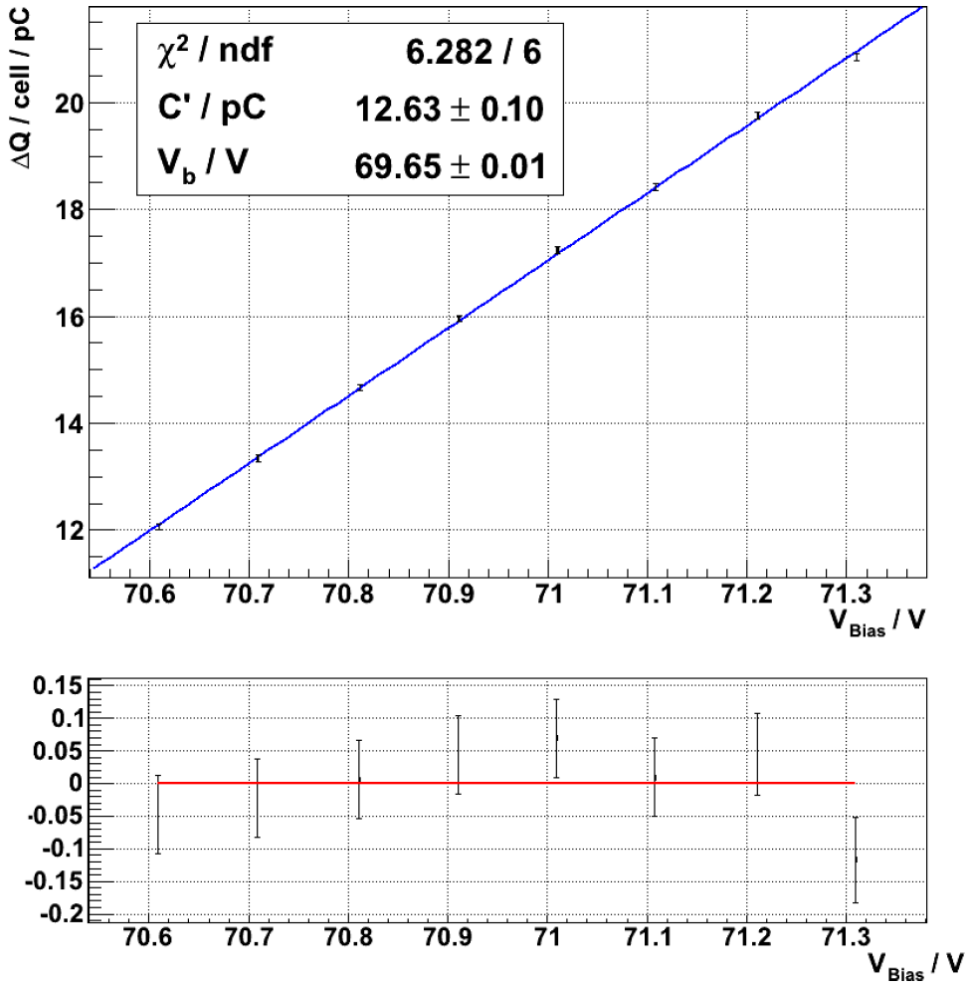

Figure 1.3: Deposited charge per fired SiPM pixel over the operating voltage at a temperature of 25 °C (SiPM-model: Hamamatsu S10362-11-100C). Plot taken from [4].

figure 1.4, its noise rate decreases for lower operating temperatures [5]. Therefore, the signal to noise ratio is better for measurements with cooled SiPMs.

To achieve cooling and temperature stabilization, the whole experiment the SiPM is used in could be set up in a specially designed refrigerator. But for very large setups this method becomes impracticable because the refrigerator's volume needs to be accordingly huge. Also, the bigger the cooled volume is, the longer it takes to reach lower operating temperatures increasing the amount of time until an experiment could be started. For long-term measurements this might not be a relevant

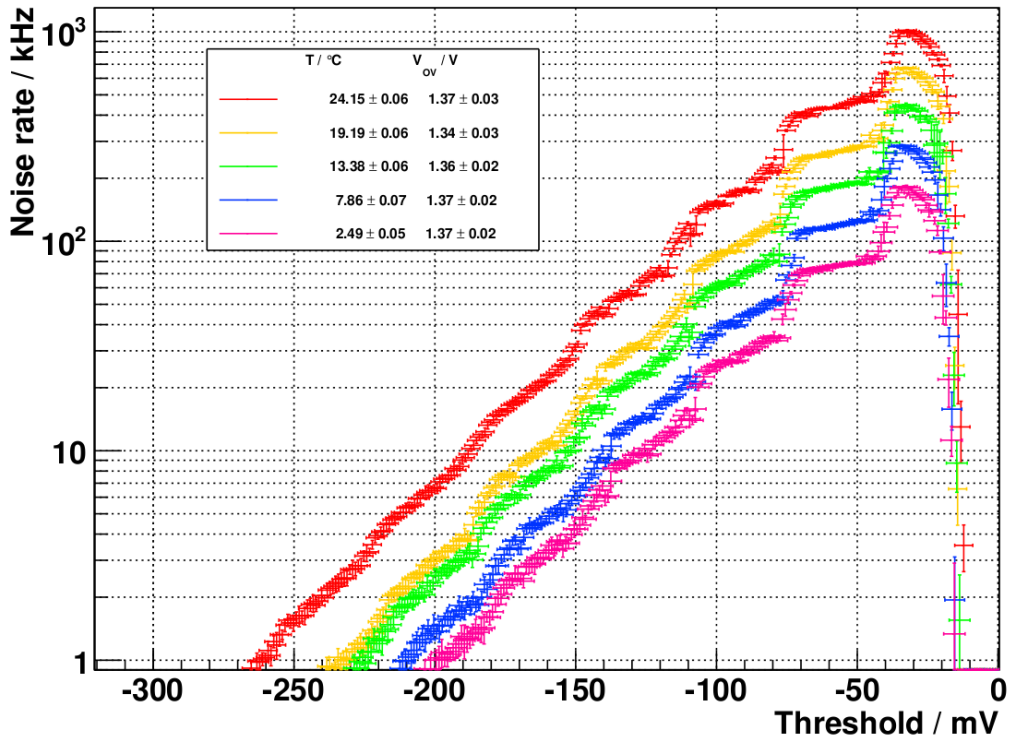

Figure 1.4: Comparison of an SiPM's noise for different temperatures (SiPM-model: Hamamatsu S10362-11-100C). Plot taken from [5]

factor, but in many cases one is interested in rather prompt results.
The approach examined in this thesis is to use a single Peltier element and a copper block with high thermal conductivity to only cool down the area around the SiPM embedded into the copper. Therefore, fast temperature regulation should be achievable.
Furthermore, the system should be automated so that an experimenter using it can focus on the measurements without having to operate the temperature stabilization as well. Because of this a PID controller mechanism is used to compute and set the needed electrical current through the Peltier element determining its cooling power.
The working principle of a Peltier element and a PID controller is described in the following chapter.

2 Theoretical Background

2.1 Peltier Effect and Peltier Elements

The Peltier effect is the consequence of the change in temperature of a contact area between different metals or between metals and semiconductors when a direct electric current flows through it. The current's direction determines whether the area heats up or cools down. So the Peltier effect is not to be confused with the Joule heating through collisions of conduction electrons with the atomic lattice of a conductor. The dependence of the Peltier heat flow Q_{Pe} on the current I is given by

$$Q_{\mathrm{Pe}} = (\Pi_{\mathrm{A}} - \Pi_{\mathrm{B}}) \cdot I \quad , \tag{2.1}$$

where $\Pi_{(\mathrm{A,B})}$ are the so called Peltier coefficients of the two joined metals or semiconductors, respectively. Among other dependences, those coefficients are functions of the temperature and the band structure of the respective materials [6],[7].
Because of the high thermal conductivity of metals, which leads to fast compensations of any temperature differences inside the metal, the Peltier effect is hard to observe in those. Semiconductors which have lower thermal conductivities, are more convenient to obtain considerable temperature differences [8]. In the following, the Peltier effect appearing in junctions between metals and n- or p-doped semiconductors is explained based on [9].
In figure 2.1 the energy band scheme is shown for a metal conductor and an n-doped semiconductor separated (a) and in contact (b). This connection is named n-metal junction.
E_{F} is the Fermi energy, q is the elementary charge and $q\Phi_{\mathrm{m}}$ and $q\Phi_{\mathrm{s}}$ stand for the metal's and semiconductor's work function which is the energy necessary for bringing an electron from the Fermi level to the vacuum. By n-doping, which creates additional energy levels near the conduction band, the semiconductor's Fermi energy is raised so that typically $\Phi_{\mathrm{m}} > \Phi_{\mathrm{s}}$.
$q\chi$ is called electron affinity and describes the gap between the energy E_{C} at the bottom of the conduction band and the vacuum energy level. The highest energy level of the valence band is labeled E_{V}.
When metal and semiconductor are brought into contact the Fermi levels align via electron diffusion from the semiconductor into the metal and the energy bands are bent until the voltage $V_{\mathrm{bi}} = \Phi_{\mathrm{m}} - \Phi_{\mathrm{s}}$ is built up inside the junction and no

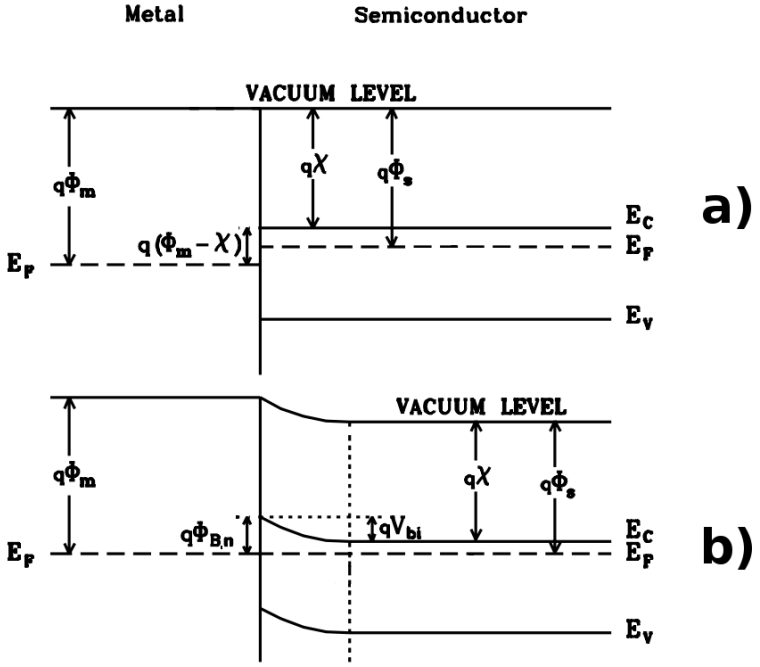

Figure 2.1: Energy band scheme for a metal and a semiconductor separeted (a) and in contact (b) forming an n-metal junction. Figure adapted from [9].

electrons can pass through anymore without an externally applied voltage.
In this state of equilibrium an electron in the metal at the Fermi level needs to overcome a barrier of

$$q\Phi_{\mathrm{B,n}} = q(\Phi_{\mathrm{m}} - \chi) \tag{2.2}$$

to bypass the gab between E_{F} and E_{C} and reach the conduction band of the semiconductor.
In our case, the work function of copper is approx. 4.65 eV and the electron affinity of the semiconductor bismuth telluride (Bi_2Te_3) is between 4.125 eV and 4.525 eV [8], [10]. Therefore, the barrier height for this junction is approx. 0.3 eV.
At temperatures on the order of 300 K thermally excited electrons can pass the junction when an external voltage is applied in a way that the semiconductor is positively charged against the metal (reverse bias). By this electron flow heat is drawn from the metal and the junction cools down. In case of an applied forward bias, an electron passing over from the semiconductor into the metal loses energy

which is released into the metal's atomic lattice as heat and the contact area warms up.

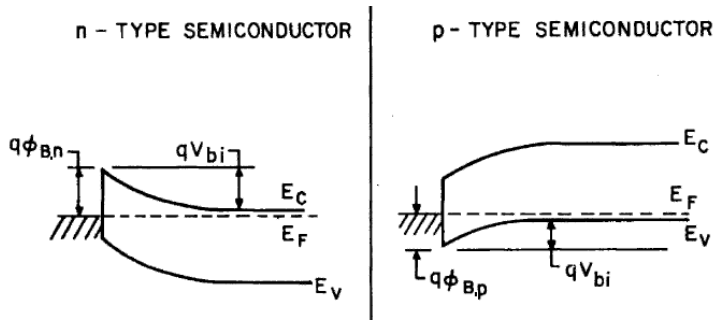

Figure 2.2: Energy band scheme for an n-metal junction and a p-metal junction without external bias voltage. Figure adapted from [9].

A similar situation shows up when a metal and a p-doped semiconductor are joined in a p-metal junction (see fig. 2.2). Those semiconductors have additional energy levels close to the valence band which lowers the Fermi energy ($\Phi_\mathrm{m} < \Phi_\mathrm{s}$). At room temperature the thermal energy of some valence electrons is high enough to reach those energy levels leaving so called holes in the valence band [11]. When the p-doped semiconductor is charged positively against the metal (forward bias), electrons that pass the junction may fill these holes, emitting energy as heat into the junction. In contrast, if a reverse bias is applied, thermally excited electrons in the valence band can overcome the barrier

$$q\Phi_\mathrm{B,p} = q\chi + (E_\mathrm{C} - E_\mathrm{V}) - \Phi_\mathrm{m} \tag{2.3}$$

and pass over into the metal section which cools down the junction [12]. For example, the gap between E_C and E_V for Bi_2Te_3 is approx. 0.2 eV [13].
As can be seen in figure 2.3, other transport processes such as electron tunneling, recombination and diffusion occur at metal-semiconductor contacts when a voltage is applied. Those processes complexly affect the current through the contact and are not discussed in this thesis. For further information see [12].

The Peltier effect can be used to build heat pumps called Peltier elements. A Peltier element consists of several semiconductor blocks (typically bismuth-telluride) connected in series by small copper layers to maximize the described effects of n- or p-metal junctions [14]. The blocks are alternately p- and n-doped and aligned in a way that the cooling and heating metal-semiconductor junctions point to different sides of the Peltier element (see fig. 2.4). The copper bridges are

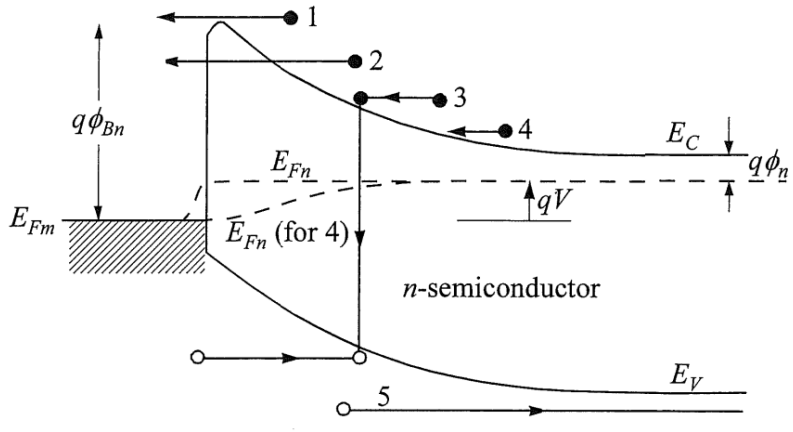

Figure 2.3: Five basic transport processes under forward bias. (1) Thermionic emmission. (2) Tunneling. (3) Recombination. (4) Diffusion of electrons. (5) Diffusion of holes. Taken from [12].

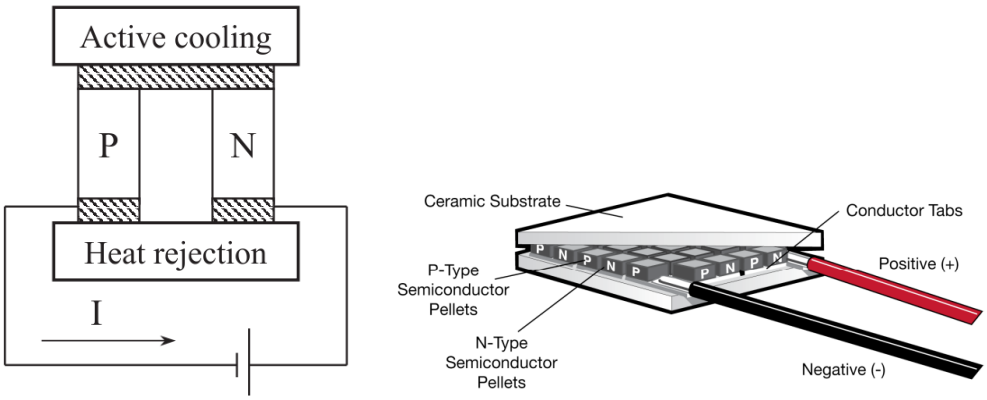

Figure 2.4: Left: Sketch of a so called thermopair composed of n- and p-doped semiconductor blocks connected by copper pads [7]. Right: Structure of a Peltier element [14].

electrically insulated by two ceramic plates which also stabilize the whole Peltier element mechanically and work as the thermal contact areas to whichever object that needs to be cooled down or heated up.

2.2 PID Controller

In the following section the basic functionality of a PID controller is explained. Further information can be found among other sources at [15].
A controller in general is a composition of three parts. Firstly, a sensor that measures the current value $i(t)$ (input) of a parameter. Secondly, a device through which this parameter can be influenced. And thirdly, an algorithm that compares the input to a desired value $s(t)$ called setpoint and computes a control variable $o(t)$ (output) based on the error function

$$e(t) = s(t) - i(t) \quad . \tag{2.4}$$

The output defines how strongly the controller interferes with the system to reach or maintain the setpoint. The newly reached value is then measured again which leads to a new value of the error function and the loop starts over.
The most basic controller is the proportional or P controller. Its output value given by

$$o(t) = k_P \cdot e(t) \tag{2.5}$$

depends only proportionally on the current error value $e(t)$. The constant k_P is named proportional gain.
The problem with a purely proportional controller is that the output value is zero for $e(t) = 0$. This means that once the setpoint is reached, the controller stops working until a certain difference between desired value and input is obtained again. This leaves the average input value systematically higher or lower than intended according to whether the setpoint is approached from above or beneath. This steady-state error can be avoided by adding a term proportional to the integral of the error function to the algorithm:

$$o(t) = k_\mathrm{P} \cdot e(t) + k_\mathrm{I} \cdot \int_0^t e(\tau)\,\mathrm{d}\tau \quad . \tag{2.6}$$

This change causes a delay in the controller's reaction because when the setpoint is acquired, the output is not immediately zero. The average input value and the setpoint match up.
Controllers using such an algorithm are called proportional-integral or PI controllers. Analogous to the proportional gain the factor k_I represents the integral gain. While a certain integral gain is needed, a rather large value of k_I severely slows down the controller leading to large fluctuations of the input value around the setpoint.
For most undisturbed systems the PI controller is enough to stabilize a certain parameter. If external disturbances are expected or cannot be excluded completely,

a third modification of the algorithm can be used to enable the controller to react to rapid changes of the input value. This change is an addition of a term proportional to the derivative of the error function:

$$o(t) = k_\mathrm{P} \cdot e(t) + k_\mathrm{I} \cdot \int_0^t e(\tau)\,\mathrm{d}\tau + k_\mathrm{D} \cdot \frac{d}{dt} e(t) \quad . \tag{2.7}$$

Such a controller is referred to as proportional-integral-derivative (PID) controller. The third parameter k_D describes the derivative gain of the algorithm. A too large value of it causes the controller to react too strongly to even the smallest changes in the input value like the noise of the used sensor. On the other hand, a small value of k_D lengthens the time that is needed to stabilize a parameter again after a disturbance from the outside.
A flow chart of how a PID controller works can be seen in figure 2.5.

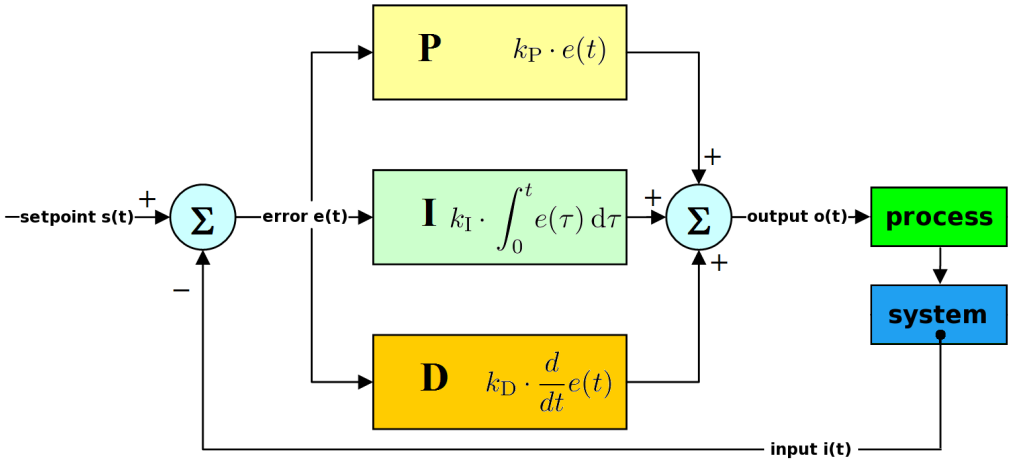

Figure 2.5: Flow chart of the PID controller functionality. Adapted from [16]

The correct set of control parameters $(k_\mathrm{P}, k_\mathrm{I}, k_\mathrm{D})$ depends strongly on the respective system. In the course of this thesis a well working set has been found manually by comparison of different combinations of parameters (see section 4.4).

3 Setup

Now that it is known how Peltier elements and PID controllers work, a setup has to be developed that combines these parts among others to a temperature stabilization system. The whole composition can be separated into three main components which are described in the following paragraphs: the cooling system that uses a Peltier element and temperature sensors to adjust and monitor the temperature of an object, a programmable current source to vary the Peltier element's power, and a microcontroller which reads out the temperature sensors, runs a PID algorithm, and controls the current source.

3.1 Cooling System

As a test object for the temperature stabilization system a small, rectangular copper block (fig. 3.2) is used. This block serves as a model for copper mountings in coming experimental setups.
The block itself is surrounded by Styrodur[1] to avoid heat conduction from the ambient air into the copper. Only the top face area is accessible where the cooling side of a Peltier element is attached. To dissipate the heat from the hot side a passive cooling element combined with a high-performance fan is mounted on top of the Peltier element.
Two temperature sensors are attached to the copper block. One on the surface opposite to the Peltier element and the other one on a lateral face next to the Peltier element. In addition to that, two more sensors which measure the ambient temperature are used as reference sensors. A heat-conductive paste is applied on the contact areas between sensors, copper block, Peltier element, and cooling element to maximize the heat transfer. A cross section scheme as well as a picture of the cooling system can be seen in figure 3.1.
The used QuickCool Peltier element (fig. 3.2) is composed of 62 doped bismuth telluride semiconductor elements (31 n-doped, 31 p-doped) [17]. The element can handle direct currents up to 8.5 A and voltages up to 3.8 V (max. power: 17.3 W) and can achieve temperature differences between the hot and the cold side of maximal 71 K. The element is connected to the current supply described in section 3.2.
The cooling element (Fischer Elektronik, model: ICK PGA 21x21, fig. 3.3) has a total of 256 aluminium cooling fins and a thermal resistance R_{th} of approx. 7 $\frac{\mathrm{K}}{\mathrm{W}}$

[1] Trademark of BASF, extruded polystyrene foam

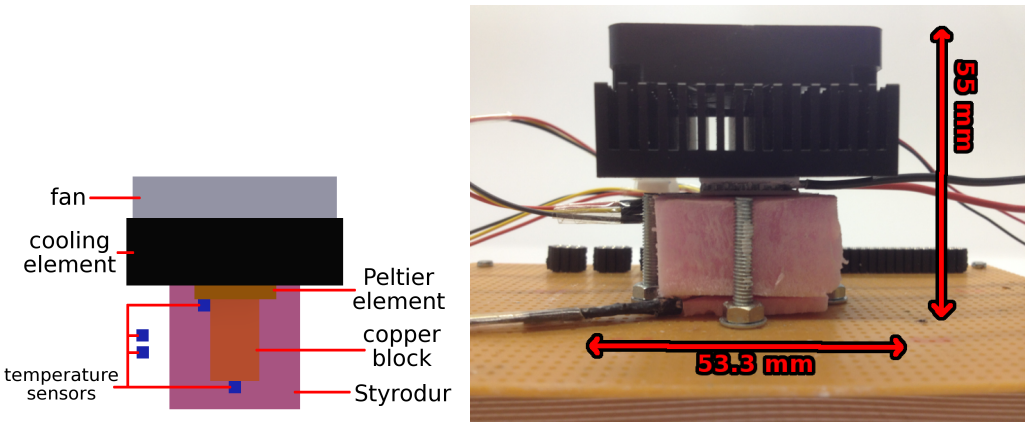

Figure 3.1: Cross section scheme and picture of the cooling system.

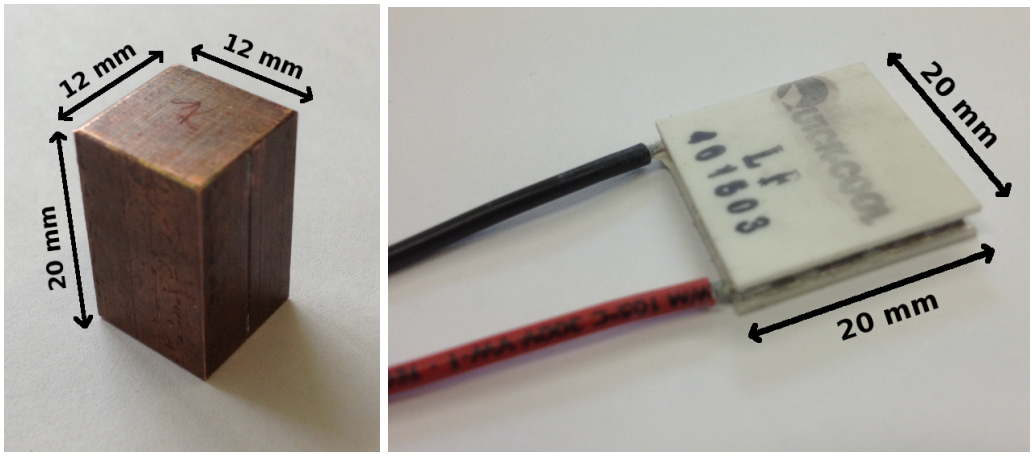

Figure 3.2: The copper block and the Peltier element used in the cooling system.

if the surrounding air is still [18]. This means that the element warms up 7 K relative to the ambient temperature while dissipating 1 W of heat. Because the Peltier element will be powered by currents up to 5 A while its resistance is about 0.5 Ω (see section 4.3), the cooling element would get very hot in the process of passively dissipating heat on the order of 10 W or would not be able to dissipate all of it. This is why the fan (SEPA, model: MFB50E05, fig. 3.3) with a maximal airflow of 10 $\frac{m^3}{h}$ is fixed on top of the cooling element to lower its thermal resistance [19]. By how much the fan increases the cooling performance will be deduced from the measurements further below (see section 4.3).
The temperatures are measured with OneWire sensors (Dallas, model: DS18B20, fig. 3.4). Their absolute accuracy is ±0.5 K for temperatures between −10 °C

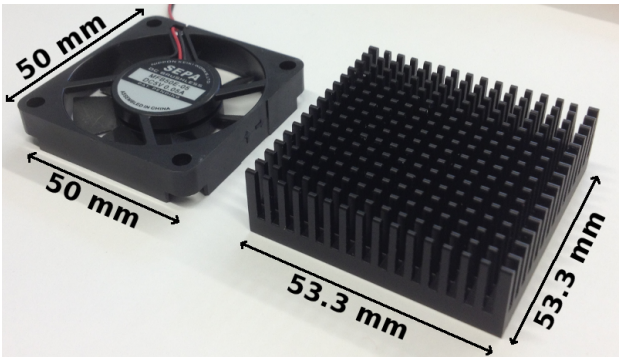

Figure 3.3: Fan and cooling element used to dissipate heat from the Peltier element's hot side.

and 85 °C and they measure with a resolution of 0.0625 °C [20]. This resolution is restricted by the program on the used microcontroller (see section 3.3) that rounds floating point numbers to two decimals by default. Therefore, the estimated uncertainty must be corrected to $\sigma_T = 0.07\,\mathrm{K}$. It takes each sensor 750 ms to convert the measured temperature into a digital signal.

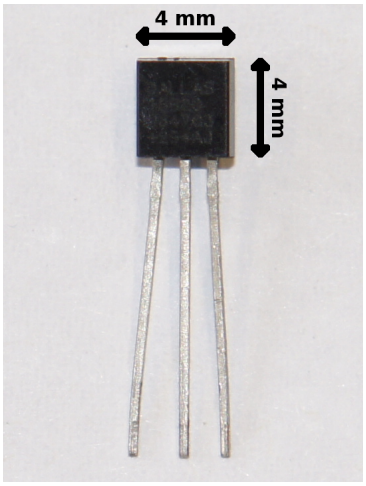

Figure 3.4: Temperatur sensor.

3.2 Programmable Current Source

To adjust automatically the electrical current through the Peltier element, the driver board "PeltierPapa" was designed in cooperation with [21] as a current

source for one or two Peltier elements controlled by a microcontroller. It can set direct currents from an external supply unit to values of 0 A to approximately 5 A with a resolution of 4 bits. This method was chosen over current control by pulse width modulation (see section 3.3) because strong fluctuating currents and the resolving current peaks could break the Peltier element when not filtered by capacitors. Also, continuously interrupted currents with a magnitude of 5 A would lead to strong noise signals which would interfere with those of the nearby SiPM and, therefore, corrupt the taken measurements.

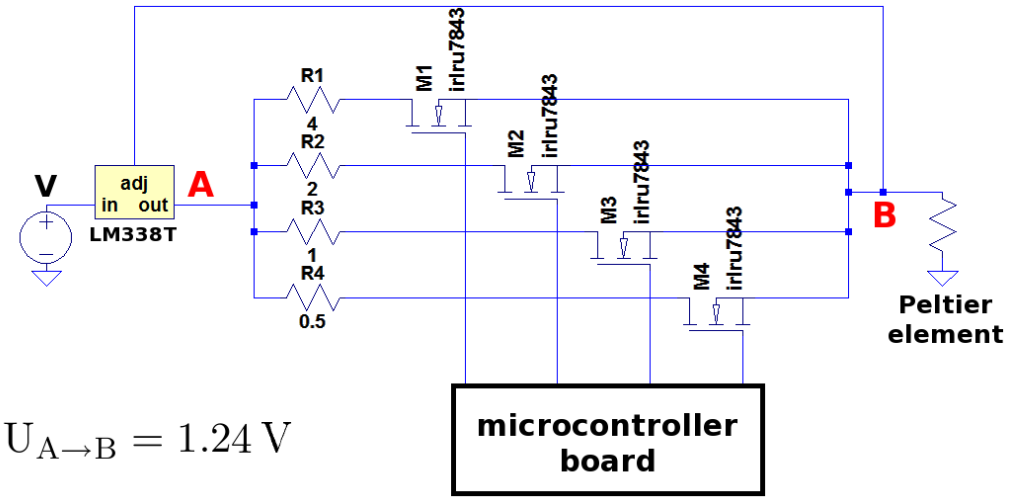

Figure 3.5: Basic elements of the adjustable current supply.

One of the basic elements of the driver board (fig. 3.5) is an LM338T voltage regulator which maintains a steady voltage of $U_{\text{ref}} = (1.24 \pm 0.05)\,\text{V}$ between the so called output and adjust pin [22]. Among those pins four resistors (conceptional values: 0.5 Ω, 1.0 Ω, 2.0 Ω and 4.0 Ω) are connected in parallel. They can be included individually into the circuit using field effect transistors (model: IRLU7843). Each of those transistors can be switched on and off by one digital pin of the used microcontroller board (see section 3.3).
Due to the fact that the 5 V provided by the pins would leave a high residual resistance inside the MOSFETs when used as their gate-source voltage, a BC550C transistor is slotted in ahead of each MOSFET's gate. The state of a transistor can be switched with a base-emitter voltage of 5 V so the microcontroller pins may be used [23]. When a transistor is inactive, the board's supply voltage of 7 V to 10 V (for one or two powered Peltier elements) is connected to the corresponding MOSFET's gate, reducing its residual resistance to about 4.0 mΩ [24]. In contrast, 5 V on the transistor's gate causes the MOSFET to inhibit. Therefore, a Schmitt

trigger (model: HEF40106) is used to invert the digital microcontroller signal [25]. This makes programming the software which converts the PID algorithm's output into the right current setting more intuitive. The driver's circuit diagram and the board design can be seen in the figures A.1 to A.3 in the appendix and the whole driver board is shown in fig. 3.6.

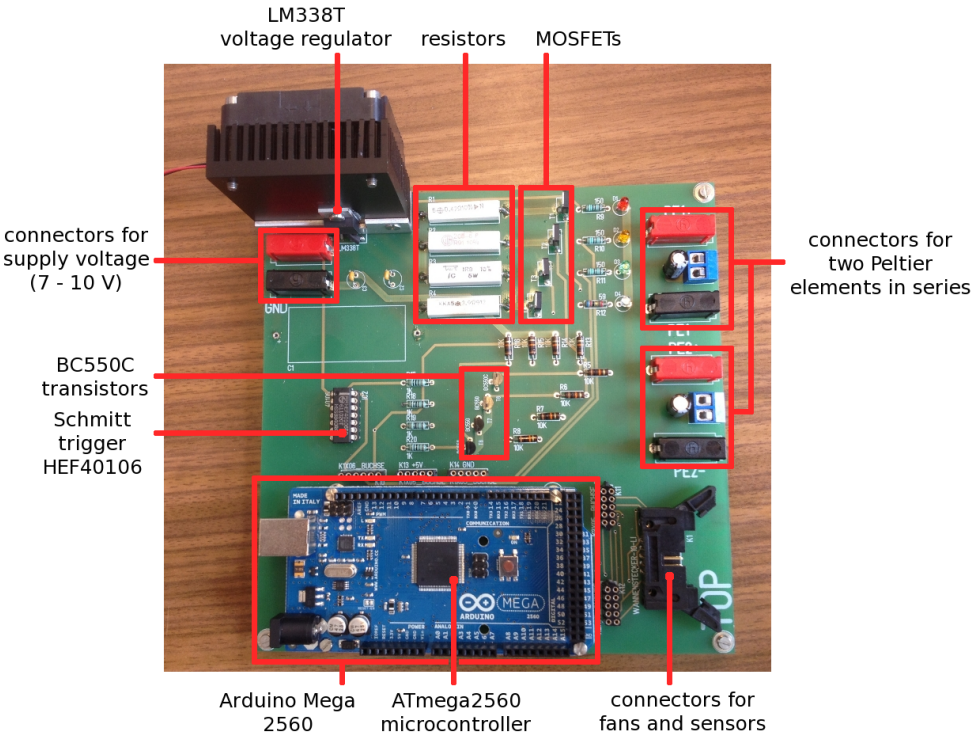

Figure 3.6: The Peltier current driver board "PeltierPapa v1.0" with mounted Arduino Mega 2560 microcontroller board.

The four resistors can be assembled to 16 different total resistances which, in combination with the constant voltage, lead to 16 current settings. Those are hereafter labelled with the numbers 0 to 15 where setting 0 means no current and 15 is the setting with the highest possible current.
To provide the board with power a Hameg HMP4040 supply unit is used. It has four programmable outputs and each of them can provide up to 10 A and 32 V (max. power 160 W) [26]. The maximum of voltage and current is adjusted to protect the driver board and the Peltier element from burning out. In the following experiments the voltage is set to 7 V while the maximum current is 5 A. The supply unit is also able to measure the actual current through each output which is used in the driver board's performance test (see section 4.2). Furthermore, a Fluke 8845A

precision multimeter is used for various measurements of currents, voltages, and resistances [27].

3.3 Microcontroller Board

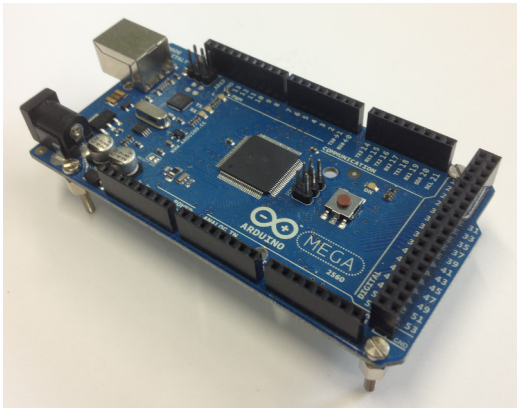

Figure 3.7: Arduino Mega 2560 microcontroller board.

To operate the adjustable current supply an Arduino Mega 2560 board (fig. 3.7) is mounted onto the driver board. It hosts an ATmega2560 microcontroller which can store up to 256 Kbyte of code using flash memory [28]. Programs are uploaded onto the microcontroller and data may be sent back to a connected computer using a USB cable. The board could be powered solely via the USB cable but to assure a steady reference voltage the Arduino is also connected to a supply unit which converts 220 V AC to 9 V DC.
The Arduino Mega 2560 has 54 digital input/output pins which operate on 5 V and have a current limit of 40 mA. The pins are either in high or low state (5 V or 0 V) and 15 of them can be controlled via pulse width modulation (PWM) as well. This means that they can be switched on and off with frequencies on the order of kHz to achieve effective voltages between 0 V and 5 V.
Six of the digital input/output pins are connected to the Schmitt trigger on the current driver board: Four of them are used to pass on the signals to the transistors while the other two serve as a power supply for the trigger. Two more pins are used to power the four OneWire sensors and recive their data. Furthermore, the fan of the cooling system is powered via two input/output pins.
The microcontroller runs a program in an infinite loop that combines three important functions: Firstly, the temperature sensors are read out simultaneously every second and their data is sent to the computer.
Secondly, a PID algorithm computes an output value using the temperature of the

copper block's side opposite to the Peltier element as the input value.
Thirdly, the output value is translated into a set of high and low states of the four pins gating the transistors.
In the course of computing the output value the input is compared to a setpoint value which can be set manually. Furthermore, the algorithm is modified to compute integer output values between 0 and 15 which represent the different settings of the current driver board.
The program code partly consists of adjusted Arduino libraries for OneWire sensors and PID controller algorithms which are available for free on the Arduino homepage[2,3].
The whole setup of the temperature stabilization system is shown in figure 3.8.

[2]http://www.arduino.cc/playground/Learning/OneWire
[3]http://www.arduino.cc/playground/Code/PIDLibrary

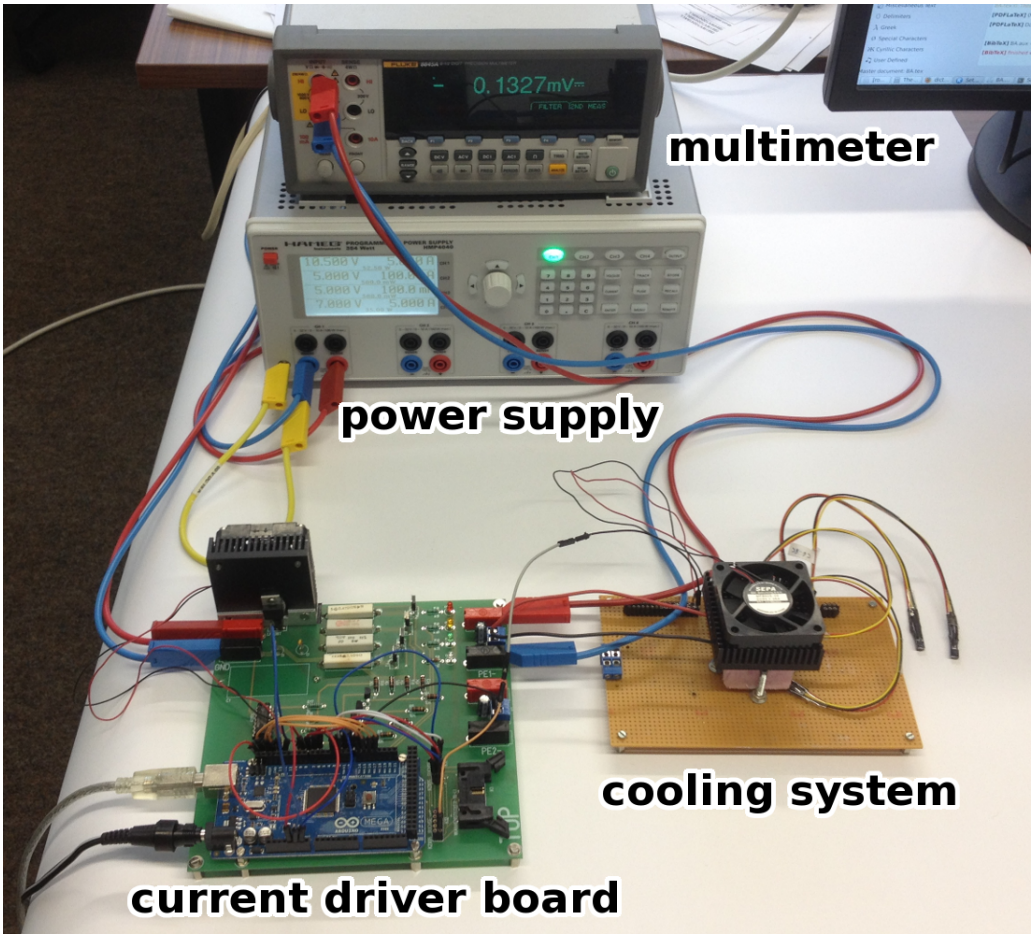

Figure 3.8: Setup of the temperature stabilization system.

4 Measurements and Results

In the course of this thesis five different experiments are conducted which are described and evaluated in this chapter.
At the beginning the used temperature sensors are calibrated to guarantee correct results for the measurements.
Following this, the current driver board's method of operating is tested by a comparison of predicted and measured Peltier currents for each of the board's settings.
In a third experiment the performance of the Peltier element and the attached cooling system is examined to figure out the limits of achievable temperatures and cooling rates.
The last two series of measurements are performed to adjust the PID controller to the setup and determine for which temperatures it can be used.

4.1 Temperature Sensor Calibration

As mentioned before, the four used sensors measure temperatures with an uncertainty of $\pm 0.5\,\mathrm{K}$ on the absolute value when the temperature is between $-10\,^{\circ}\mathrm{C}$ and $85\,^{\circ}\mathrm{C}$. To minimize this offset between real and measured temperature, one would have to calibrate each sensor under laboratory conditions. That is not only time-consuming and complicated, but also unnecessary for the experiments conducted in the course of this bachelor's thesis. As will be shown later, the stabilization system is insensitive for small changes in temperature. Meaning that if it works for a given setpoint temperature T, it will work just as well for temperatures $T' \in [T - 0.5\,\mathrm{K}, T + 0.5\,\mathrm{K}]$. This is why for the following experiments the uncalibrated absolute accuracy works well.
However, one has to keep in mind that the absolute accuracy is important for further measurements with SiPMs and, therefore, sensors used in those experiments have to be calibrated precisely.
In contrast to the absolute values, the temperature difference between two sensors must be measured correctly within their resolution of $\sigma_T = 0.07\,\mathrm{K}$. To achieve this, a constant offset for each sensor has to be derived. This offset has to be subtracted from its signal, so that all sensors would provide the same value when placed in a medium of one temperature. The offsets refer to the arithmetic mean of all four sensor signals.
The setup for this relative calibration is simple: the sensors are placed next to each other in a block of Styrodur so that the temperature fluctuation is small and

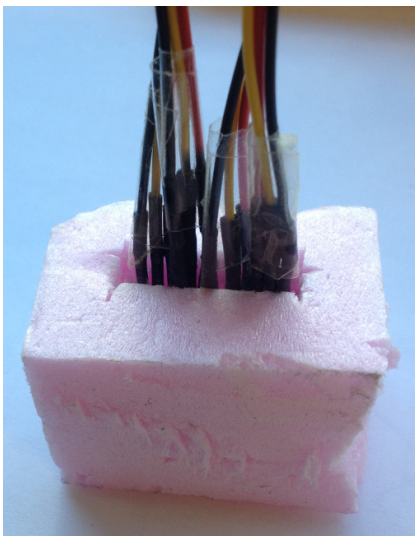

Figure 4.1: The used temperature sensors brought together in a block of Styrodur for the calibration.

the temperature is approximately the same for all four sensors (see fig. 4.1). The microcontroller board powers the sensors, reads them out every second for about 20 minutes, and sends the data to a computer via USB where it is saved in a text file.
For every second i the deviations $\Delta T_j^{(i)}$ of the four signals $T_j^{(i)}$ (j represents the sensors 1 to 4) from the arithmetic mean $\overline{T}^{(i)}$ are calculated as follows:

$$\Delta T_j^{(i)} = T_j^{(i)} - \overline{T}^{(i)} \quad , \quad \overline{T}^{(i)} = \sum_{j=1}^{4} T_j^{(i)} \quad . \tag{4.1}$$

The calculated values are filled into one histogram per sensor. As an example, the histogram for sensor 2 is shown in figure 4.2.
The mean values of those histograms are the offsets ΔT_j that correct the measured values so that

$$T_j = T_j' - \Delta T_j \tag{4.2}$$

where T_j' is the measured temperature and T_j is the calibrated value.
Because the uncertainty on the mean value is very small for over 1200 entries, the RMS value is taken as the uncertainty $\sigma_{\Delta T_j,\mathrm{RMS}}$ on ΔT_j. The results are shown in table 4.1.
As for each of the sensors $\sigma_{\Delta T_j,\mathrm{RMS}}$ is much smaller than its resolution, the uncer-

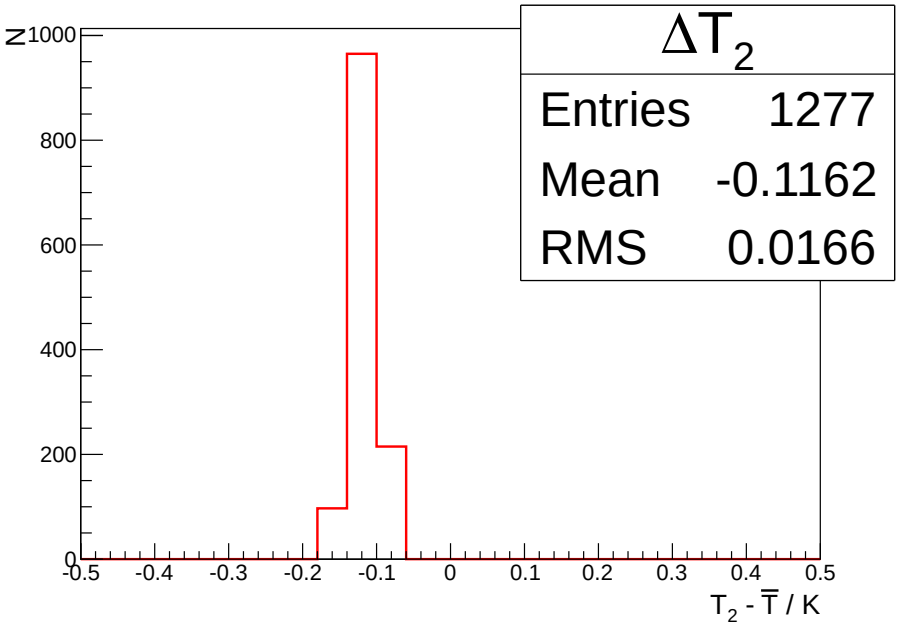

Figure 4.2: Histogram of deviations between the temperatures measured by sensor 2 and the mean value of all four used temperature sensors.

tainty of one measurement of temperature will still be estimated with $\sigma_T = 0.07\,\mathrm{K}$. Uncertainties of temperature differences are therefore $\sigma_{\Delta\mathrm{T}} = \sqrt{2} \cdot \sigma_{\mathrm{T}} = 0.10\,\mathrm{K}$. These calibration constants will be applied to all following measurements and the errors will be handled accordingly.

sensor	ΔT_j / K	$\sigma_{\Delta T_j,\mathrm{RMS}}$ / K
1	−0.017	0.020
2	−0.116	0.017
3	+0.003	0.017
4	+0.130	0.017

Table 4.1: The offsets used to correct the measured values of the four temperature sensors in course of the relative calibration.

4.2 Test of the Current Driver Board's Performance

To verify the driver board's method of operating, the current I_{pre} through the Peltier element for each setting is predicted based on the corresponding total resistance of the resistor assembly and the reference voltage $U_{\text{ref}} = (1.24 \pm 0.05)\,\text{V}$ of the LM338T. These values are compared to the measured currents I_{exp}.
In the course of calculating I_{pre}, the four resistances are measured with the help of the Fluke multimeter. Due to fluctuations in the displayed values, $\sigma_{R'} = 0.01\,\Omega$ is the estimated uncertainty for a given resistance value. The resistances of the used cables and test prods are determined and subtracted to correct the resistance values. Therefore, the uncertainty of the four corrected resistances is $\sigma_R = \sqrt{2} \cdot \sigma_{R'} = 0.014\,\Omega$. The results are listed in tab. 4.2.

Resistor	Resistance	Uncertainty
R_1	$0.500\,\Omega$	$\pm 0.014\,\Omega$
R_2	$0.900\,\Omega$	
R_3	$1.780\,\Omega$	
R_4	$3.920\,\Omega$	

Table 4.2: Resistances of the four ohmic resistors used on the Peltier element driver board (after correction).

With the formula for the total resistance in parallel connections and Ohm's law,

$$\frac{1}{R_{\text{tot}}} = \sum_i \frac{1}{R_i} \quad \text{and} \quad I_{\text{pre}} = \frac{U_{\text{ref}}}{R_{\text{tot}}} \quad , \tag{4.3}$$

I_{pre} for different driver board settings is predicted. The uncertainty $\sigma_{I_{\text{pre}}}$ is found with the help of the error law of Gauss using $\sigma_{U_{\text{ref}}}$ and σ_R.
The actual Peltier currents I_{exp} are measured with an estimated uncertainty of $\sigma_{I_{\text{exp}}} = 0.5\,\text{mA}$. Again, this estimation is based on fluctuations of the displayed values.
The comparison between I_{exp} and I_{pre} is shown in figure 4.3 and table 4.3.

All the values match the prediction within their uncertainties which shows that the driver board works well in the desired range of 0 A to 5 A with step sizes of approximately 300 mA. The fact that the different current settings are not exactly equidistant is because of the four resistances that differ from the values the board was designed with. The results also show that the conversion between setting number and resistor composition is implemented correctly into the microcontroller's program code.

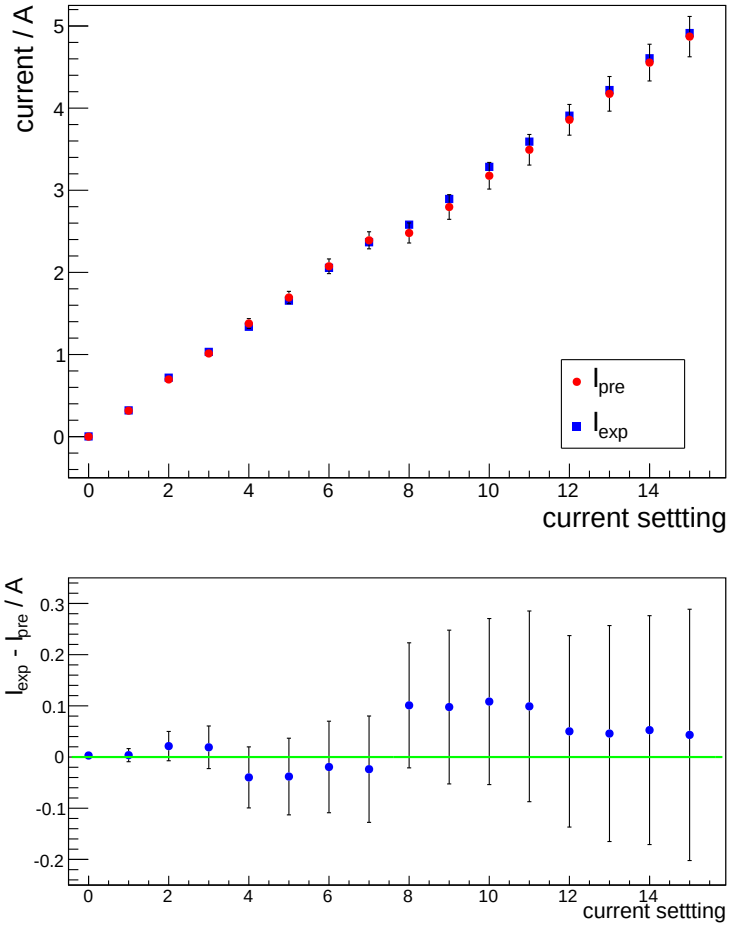

Figure 4.3: Top: Predicted (red) and measured (blue) values of currents through the Peltier element depending on the setting of the current source. Bottom: Residual plot.

4.3 Test of the Cooling System's Performance

For these measurements the copper block is removed from the setup and a temperature sensor is placed directly onto the cold side of the Peltier element. Another sensor is fixed on the cooling element right next to the Peltier element so its measured temperature is approximately the same as the one on the hot Peltier element side. Both sensors, the Peltier element, and the bottom of the cooling element are embedded into Styrodur to preserve the parts from heat conduction from the

setting	R_{tot} / Ω	I_{pre} / A	I_{exp} / A	ΔI / A
0	–	0.00	0.00	0.00
1	3.92	0.32	0.32	0.00
2	1.78	0.70	0.72	0.02
3	1.22	1.01	1.03	0.02
4	0.90	1.38	1.34	−0.04
5	0.73	1.69	1.66	−0.03
6	0.60	2.07	2.06	−0.01
7	0.52	2.39	2.37	−0.02
8	0.50	2.48	2.58	0.10
9	0.44	2.80	2.89	0.09
10	0.39	3.18	3.29	0.11
11	0.36	3.49	3.59	0.10
12	0.32	3.86	3.91	0.05
13	0.30	4.17	4.22	0.05
14	0.27	4.55	4.61	0.06
15	0.25	4.87	4.91	0.04

Table 4.3: List of the total resistances for each current driver board setting as well as the calculated and measured currents through the connected Peltier element and their difference.

outside. A third sensor measures the room temperature as a reference. Figure 4.4 shows a cross section scheme of the setup.

Figure 4.4: Cross section scheme of the setup used for the performance test of the cooling system.

In the course of this performance test, the PID controller is turned off and the settings of the current driver board are adjusted manually. For each setting the Peltier element is powered for about 180 seconds. The sensors measure the tem-

peratures T_{cold} on the element's cold side, T_{hot} on the hot side, and the ambient temperature T_{ref} every second.
Furthermore, current I and voltage U at the Peltier element are measured to determine its electrical power P and resistance R. The uncertainties on those values are estimated individually for every measurement based on small fluctuations in the displayed results of the ampere- and voltmeter.

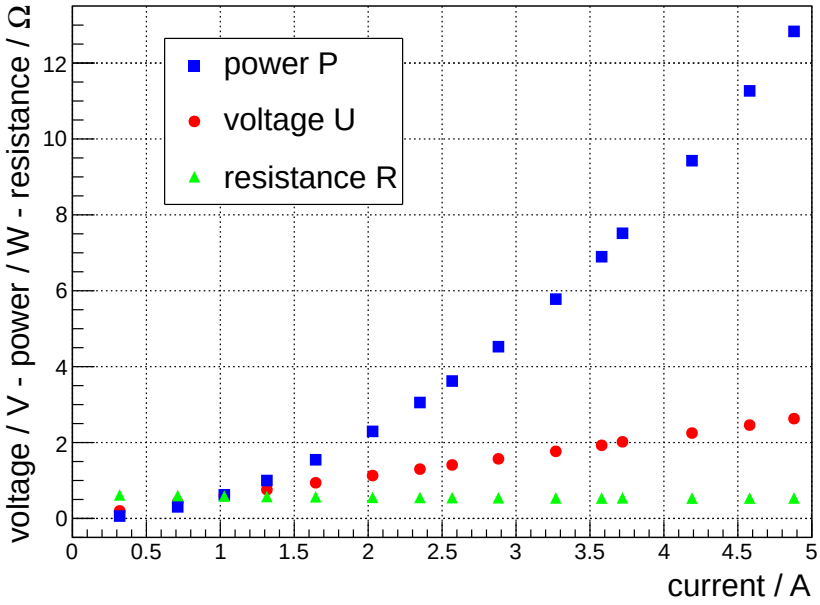

Figure 4.5: The Peltier element's electrical power and resistance as well as the voltage as function of the applied current.

The electrical power and resistance of the Peltier element are calculated using

$$P = U \cdot I \quad \text{and} \quad R = \frac{U}{I} \quad . \tag{4.4}$$

In figure 4.5 those values and the measured voltages are shown plotted against the electrical current for each driver board setting.
The resistance of the Peltier element appears to stay almost constant at approx. $0.5\,\Omega$ which means that it can be seen as a purely ohmic resistor. As we expect for an ohmic resistor, the Peltier element's electrical power shows an approximately quadratic dependence on the current strength while the voltage follows linearly.
As an example, the courses of the three measured temperatures as well as the temperature difference between the Peltier element's cold and hot side are shown

for the current settings 4 and 14 in figure 4.6.

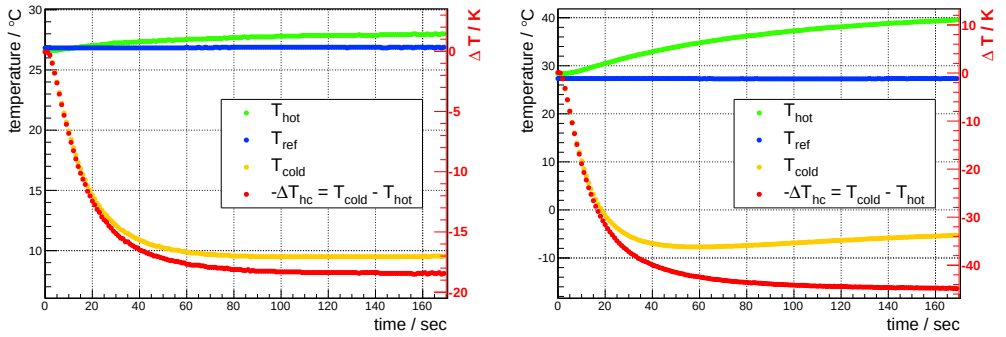

Figure 4.6: Comparison of the temperatures T_{cold} and T_{hot} on both sides of the Peltier element, the difference ΔT_{hc} between them as well as the room temperature T_{ref} as function of the time for the current settings 4 (left) and 14 (right).

As expected, higher electrical currents lead to lower temperatures T_{cold} at the cooling side and larger gaps ΔT_{hc} between cold- and hot-side temperature in the same amount of time.
But while T_{cold} reaches a stable value during the measurement for the lower current setting, the cold side of the Peltier element slowly warms up again towards the end of the observation when powered with currents close to the limit of the driver board. This indicates that the cooling element and the fan do not dissipate the heat effectively enough from the hot side of the Peltier element and heat is being conducted from the hot to the cold side.
The lack in heat dissipation can also be seen in the rise of T_{hot} during the measurement with the higher current.
As the warming is a very small and slow effect and considering that it is mentionable only for cold-side temperatures below freezing point, which are not of interest for the setup, the cooling system appears to be well suited for the following experiments.
To examine how fast the Peltier element's cold side can cool down depending on the current, the cooling rate $v_{\mathrm{cold},i}$ for each second i is calculated by dividing the difference between the temperatures one second after and before by the time difference of 2 seconds:

$$v_{\mathrm{cold,i}} = \frac{T_{\mathrm{cold,i+1}} - T_{\mathrm{cold,i-1}}}{2\,\mathrm{sec}} \quad . \tag{4.5}$$

Beside the highest cooling rates $v_{\mathrm{cold}}^{\mathrm{max}}$, the lowest cold-side temperatures $T_{\mathrm{cold}}^{\mathrm{min}}$,

and the largest temperature differences $\Delta T_{\mathrm{hc}}^{\mathrm{max}}$ between hot and cold side are determined for each current setting. The results are shown in table 4.4.

#	I / A	P / W	$T_{\mathrm{cold}}^{\mathrm{min}}$ / °C	$\Delta T_{\mathrm{hc}}^{\mathrm{max}}$ / K	$v_{\mathrm{cold}}^{\mathrm{max}}$ / $\frac{\mathrm{K}}{\mathrm{s}}$
1	0.32	0.06	21.49	5.20	−0.22
2	0.71	0.31	16.12	10.94	−0.50
3	1.03	0.62	12.30	15.01	−0.71
4	1.32	1.00	9.49	18.51	−0.88
5	1.65	1.55	6.49	22.26	−1.06
6	2.03	2.29	3.37	26.07	−1.28
7	2.35	3.06	1.30	29.01	−1.44
8	2.57	3.62	0.24	31.00	−1.53
9	2.88	4.53	−1.75	33.50	−1.66
10	3.27	5.78	−3.75	36.44	−1.88
11	3.58	6.90	−4.94	38.63	−1.97
12	3.72	7.51	−5.81	40.43	−2.06
13	4.19	9.43	−6.88	42.69	−2.22
14	4.58	11.27	−7.69	44.88	−2.31
15	4.88	12.83	−8.00	46.50	−2.40

Table 4.4: A list of the lowest achievable temperatures on the cold side of the Peltier element and the highest differences between this and the hot side as well as the highest cooling rates for the different current settings.

Without the copper block attached, the cooling system can achieve temperatures down to −8.00 °C and temperature differences up to 46.50 K. These results suggest that suitable temperatures for working with SiPMs can be realized even with an additional volume like the copper block that has to be cooled, too.
Furthermore, the cooling rates of maximal $-2.40\,\frac{\mathrm{K}}{\mathrm{s}}$ show that low temperatures can be achieved within a couple of seconds which justifies the use of the chosen Peltier element for a fast temperature stabilization and cooling system.
To examine the cooling system's performance in dependence on the supplied power, the saturation values $T_{\mathrm{cold}}^{\infty}$, $T_{\mathrm{hot}}^{\infty}$, and $T_{\mathrm{ref}}^{\infty}$ of the three temperatures as well as the differences $\Delta T_{\mathrm{hc}}^{\infty}$, $\Delta T_{\mathrm{rc}}^{\infty}$, and $\Delta T_{\mathrm{hr}}^{\infty}$ between them are determined for each of the 15 measurements. If no saturation is reached, the temperature values approached at the end of an observation are taken. These are plotted against the Peltier element's electrical power. The resulting graphs are shown in figures 4.7 and 4.8. The reference temperature $T_{\mathrm{ref}}^{\infty}$ stays almost constant providing comparability of the measurements. Apart from this, it can be seen that $T_{\mathrm{cold}}^{\infty}$ approaches a constant value of approx. −5.00 °C for high electrical powers while $T_{\mathrm{hot}}^{\infty}$ keeps rising up

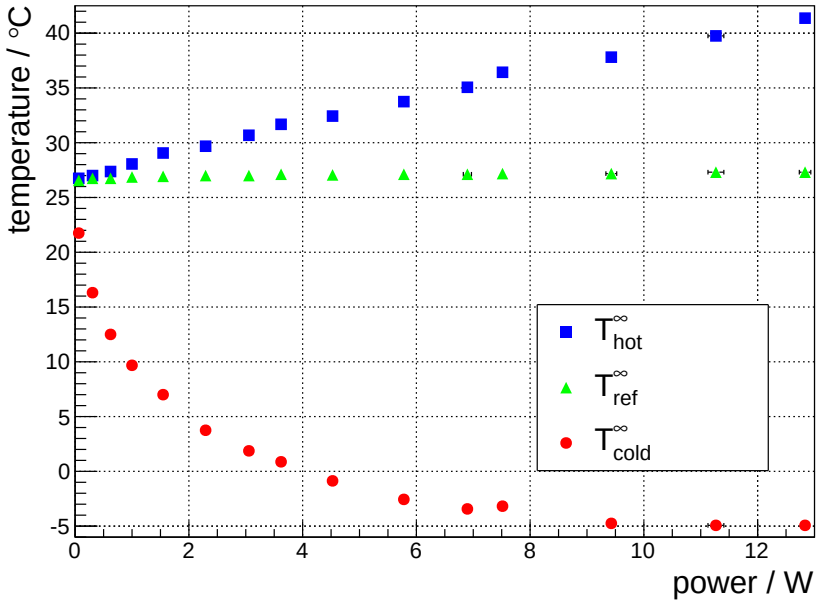

Figure 4.7: Saturation values of the three measured temperatures towards the end of each observation over the electrical power on the Peltier element.

almost linearly. So from a certain point onwards adding more power does not cool the cold side of the Peltier element any further but merely heats the hot surface.

Similar to that, fig. 4.8 shows that the temperature difference $\Delta T_{\mathrm{rc}}^{\infty}$ between the room temperature and the cold-side temperature saturates at roughly 32 K even though it is possible to achieve increasing gaps $\Delta T_{\mathrm{hc}}^{\infty}$ between both sides of the Peltier element with higher powers. The gain in reachable temperature differences gets smaller towards the limits of the current driver board and describes the Peltier element's cooling performance

$$C_i = \frac{\Delta T_{\mathrm{hc},i}^{\infty} - \Delta T_{\mathrm{hc},i-1}^{\infty}}{P_i - P_{i-1}} \tag{4.6}$$

where i is the power setting.

The cause of the stagnation of $\Delta T_{\mathrm{rc}}^{\infty}$ is the constant rise of the cooling element's temperature $\Delta T_{\mathrm{hr}}^{\infty}$ relative to the ambient temperature which is almost linear to the power. It's thermal resistance $R_{\mathrm{th},i}$ at each power setting i can be calculated using

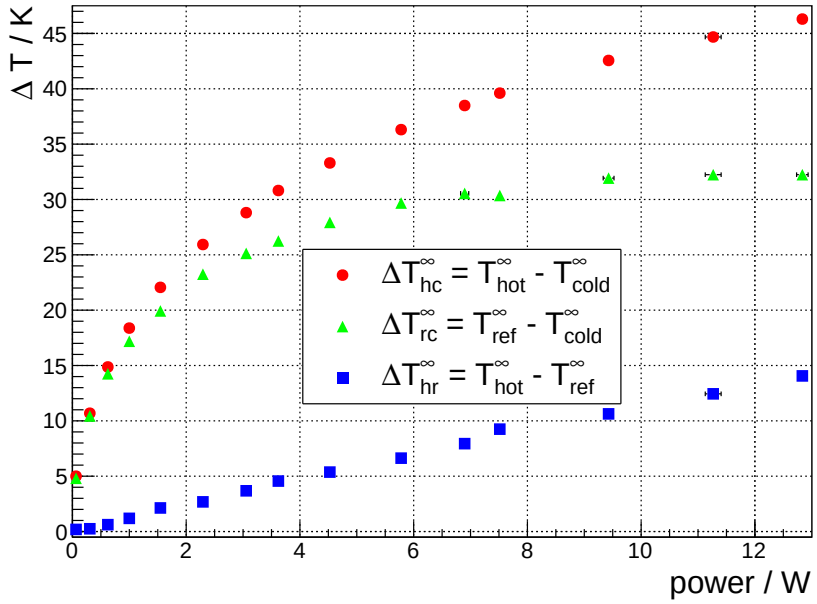

Figure 4.8: Differences between the saturation temperatures in dependence of the power setting they have been reached with.

$$R_{\mathrm{th},i} = \frac{\Delta T^{\infty}_{\mathrm{hr},i}}{P_i} \quad . \tag{4.7}$$

In figure 4.9 both the cooling performance and the thermal resistance are shown as a function of the power. The plot shows that the thermal resistance is almost constant for all current settings with an average value of approximately 1.2 $\frac{\mathrm{K}}{\mathrm{W}}$. In comparison to the thermal resistance of the passive cooling element alone ($R_{\mathrm{th}} = 7$), the mounted fan improves its performance by a factor of about 6.

The plot also reveals that the Peltier element's cooling performance lines up and then drops slightly below the thermal resistance of the cooling system for the two highest power settings. This means that any additional power given to the Peltier element heats the cooling element by the same amount as it increases the difference between cold- and hot-side temperature. In this case the temperature difference $\Delta T^{\infty}_{\mathrm{rc}}$ between the cold side of the Peltier element and the surrounding air cannot be increased any more. This corresponds to the results taken from plots 4.7 and 4.8.

In the course of achieving even lower temperatures with the given Peltier element, the crossing of C and R_{th} has to be shifted to higher powers by lowering the thermal

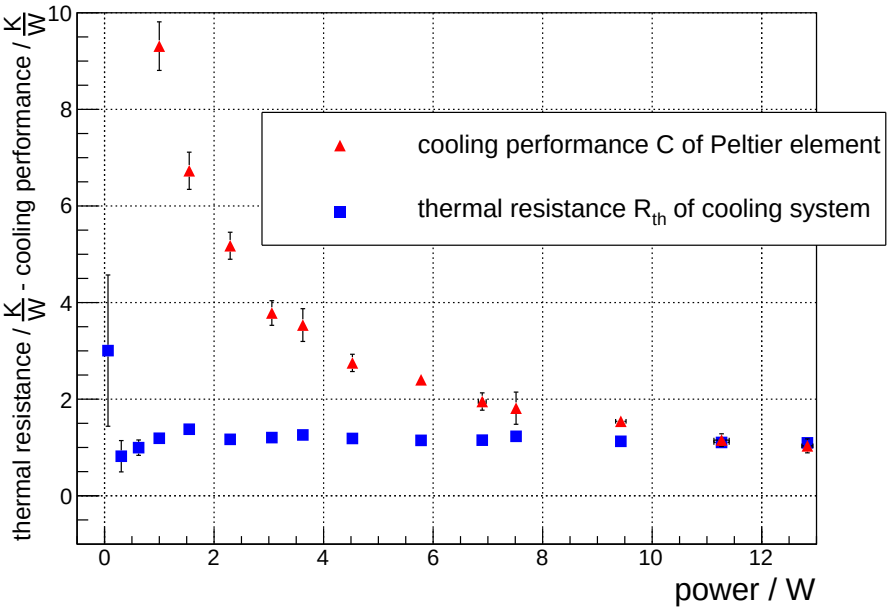

Figure 4.9: Cooling performance of the Peltier element and the thermal resistance of the combination of cooling element and mounted fan over the Peltier element's electrical power.

resistance. That could be accomplished by using stronger fans or a completely different system such as water cooling.
The lowest reachable temperature is also limited by the Peltier element itself because it can only handle powers up to approx. 17 W and the gain in $\Delta T_{\mathrm{hc}}^{\infty}$ is merely approx. $1.2\,\frac{\mathrm{W}}{\mathrm{K}}$ for the highest power setting. This means that for a little increase in the temperature difference the element would have to be powered at its absolute upper limits rendering the whole setup unreliable. So the Peltier element would have to be exchanged by a more powerful one and another current driver board would have to be designed, too.
However, for working with SiPMs the cooling system turned out to be adequate.

4.4 Adjustment of the PID Controller

Since the right combination of control parameters $(k_{\mathrm{P}}, k_{\mathrm{I}}, k_{\mathrm{D}})$ is different for every observed system and method that is used to reach the setpoint, a useful parameter set for the test setup cannot be calculated per se. Regarding the uniqueness of the controller at hand including the "PeltierPapa" driver board, the right parameters

cannot be estimated based on a comparison to a similar setup. This is why in this case a working set is determined via careful examination of various parameter combinations at a constant setpoint temperature $T_{\text{set}} = 10.12\,^{\circ}\text{C}$.
Since strong disturbances in the copper block's temperature other than those induced by the Peltier element are not expected for this setup, the derivative gain k_{D} should be small in comparison to the other two gains. So in this test it is switched between 0 (PI controller) and 1 (PID controller).
Besides this, the control algorithm should react strongly to the difference between setpoint and copper block temperature so that great gaps are closed quickly and the setpoint temperature is approached within a reasonable amount of time. Therefore, the values 2 and 5 are tested for the proportional gain k_{P}. The integral gain k_{I} is tested with the values 2 and 5, too. All eight combinations of the chosen parameters are examined.
Every series of measurements takes about 300 seconds and is started by setting a different combination of PID parameters and turning on the external power supply allowing the temperature stabilization system to start working. Every second the temperature sensors are read out by the microcontroller board and their data is sent to the PC.
Using the temperature T_{in} of the sensor opposite to the Peltier element as the input value, a new output is computed by the PID algorithm which is then used to set the Peltier element current via the driver board.
The room temperature T_{ref} is held roughly constant over the period of the measurements for two reasons: Firstly, the results would not be comparable when one measurement is affected by disturbances in the ambient temperature more than the others. And secondly, the controller might work differently for equal parameters but varying differences ΔT between the mean ambient temperature and the setpoint temperature:

$$\Delta T = \overline{T_{\text{ref}}} - T_{\text{set}} \qquad , \qquad \overline{T_{\text{ref}}} = \sum_i T_{\text{ref},i} \quad . \tag{4.8}$$

The chosen criterion for a stabilized temperature is, that the occupied temperature must not differ more than two units of the sensor's resolution from the setpoint temperature to each side so that the maximal deviation is $\pm 0.14\,\text{K}$. The time at which this criterion is fulfilled is labeled t_{stable} and is used to compare the quality of different parameter settings.

The results for the eight different parameter settings can be found in tab. 4.5. As shown, the temperature difference ΔT between setpoint temperature and average room temperature only changes between $17.52\,\text{K}$ and $17.65\,\text{K}$ enabling us to directly compare the measurements. It can also be seen that only four settings result in a stable temperature before the end of the measurement.

$(k_\mathrm{P}, k_\mathrm{I}, k_\mathrm{D})$	t_stable / s	ΔT / K
$(2, 5, 0)$	–	17.55
$(2, 5, 1)$	–	17.53
$(2, 2, 0)$	–	17.52
$(2, 2, 1)$	271	17.54
$(5, 2, 1)$	138	17.58
$(5, 2, 0)$	175	17.65
$(5, 5, 0)$	–	17.61
$(5, 5, 1)$	216	17.55

Table 4.5: List of stabilization times and the difference between setpoint and average room temperature for different control parameter settings.

The best results are achieved with the parameter set $(5, 2, 1)$ with 138 s until the stabilization is accomplished (see fig. 4.10). The residual plot in figure 4.11 shows the deviations $T_\mathrm{in} - T_\mathrm{set}$ from t_stable until the end of the measurement. The green shading shows the $\pm 2\sigma_T$-area in which the stabilization criterion is fulfilled.

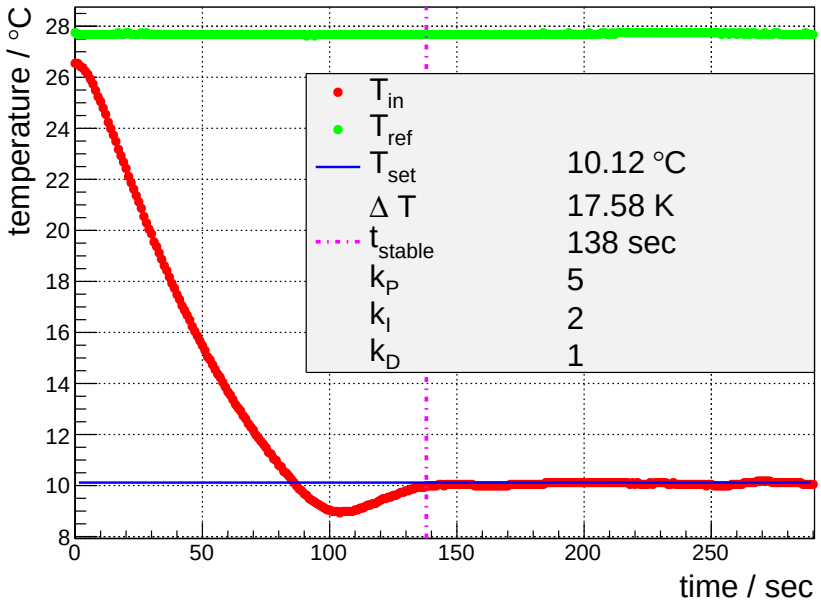

Figure 4.10: Temperature course for the parameter set (5,2,1).

It must be said that this parameter set is not necessarily the ideal one for this

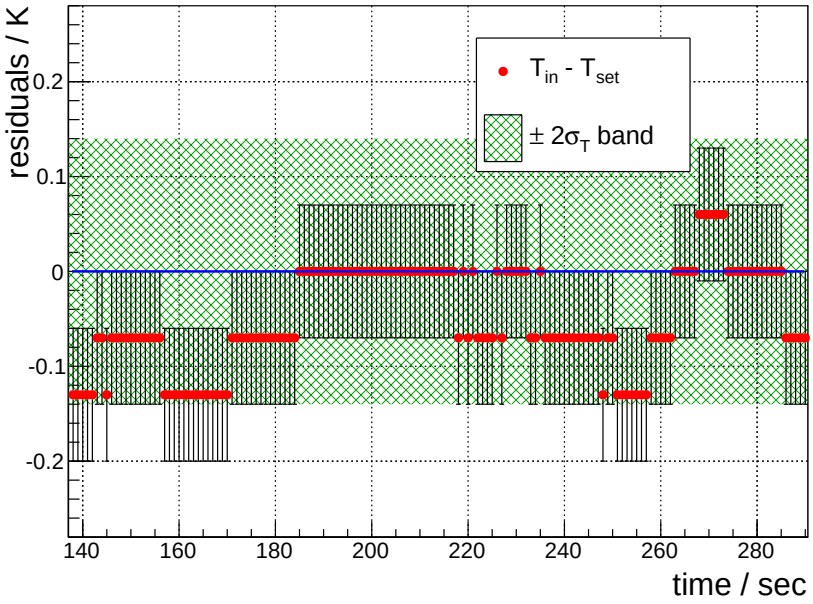

Figure 4.11: Residual plot of the temperature course after stabilization is achieved for the parameter set (5,2,1).

setup, it is merely the best set out of the eight tested compositions. For even better solutions the parameters k_P, k_I and k_D could be varied in smaller steps and/or a greater range of possible values. But considering that n different values per parameter result in n^3 measurements, this method would rapidly lead to a very long time to test all settings. In this case that would be unnecessary because a few seconds more or less until temperature stabilization are not significant as long as it is reached within a short time and maintained afterwards. The parameter set $(5, 2, 1)$ fulfills these conditions.

It is promising to see that temperature stabilization is achievable with the given setup because it suggests that comparable systems can be stabilized as well. But since the PID parameters for this system differ from those used in other experiments, it is more important to examine in which way changing the gains affects the controller's behavior. For this reason two settings are compared for each of the three gains in which the value of the examined gain is changed while the other two are held constant.

As can be seen in figure 4.12, setting the derivative gain to 0 averts a stabilization before the end of the measurement. The course of the temperature T_in suggests, that even without the algorithm's derivative term a stable temperature may be

achieved, but it would take much longer than in the case of $k_\mathrm{D} = 1$.

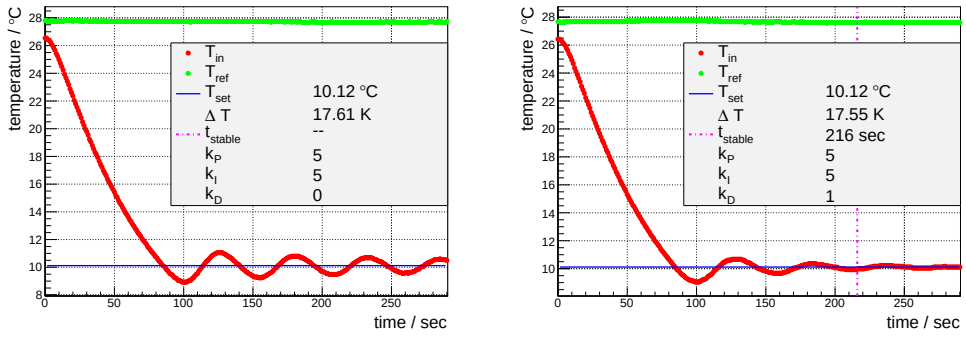

Figure 4.12: Comparison of two two controller settings with different derivative gain k_D.

The plots in figure 4.13 show the consequences of changing the integral gain. As suspected the higher value of k_I leads to large oscillations (approx. $^{+2}_{-1}$ K) of T_in around the setpoint temperature which do not appear to decrease over time. The controller reacts too slowly to the actual difference between measured and desired temperature.
The smaller integral gain eventuates in temperature stabilization towards the end of the measurement. The temperature still fluctuates at the beginning but the deviations get smaller with each oscillation.

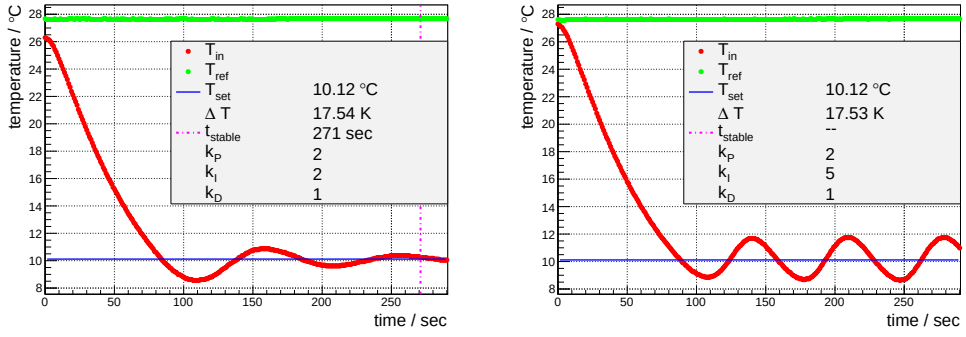

Figure 4.13: Comparison of two two controller settings with different integral gain k_I.

These oscillations can be damped even stronger when the controller's proportional gain is set to a higher value than the integral gain (see fig. 4.14). In contrast to that, the smaller value of k_P prevents T_in from being stabilized during the

observation.

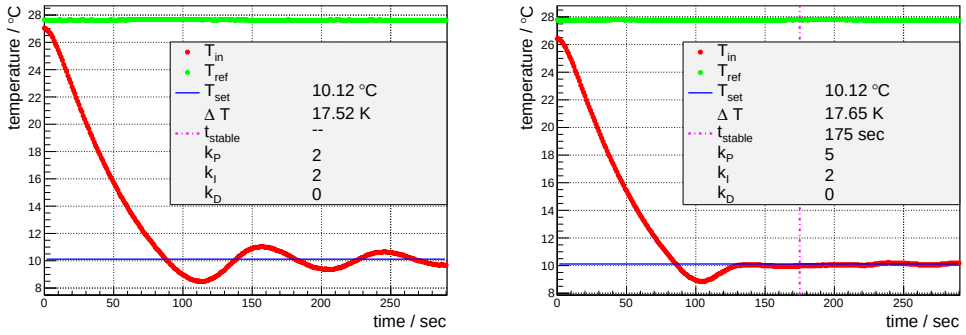

Figure 4.14: Comparison of two controller settings with different proportional gain k_P.

The conclusions found through the comparison of different parameter settings and the resulting behaviour of the controller can be put to use when it comes to adjusting the PID controller to a different but comparable experimental setup.

4.5 Variation of the Setpoint Temperature

Now that a working set of PID parameters has been found, the setpoint temperature is varied to examine whether and how strongly the control parameters depend on the difference between setpoint temperature and ambient temperature.
Beginning with a setpoint temperature of 27.62°C and decreasing this value by 2.50°C each time, 12 series of measurements are taken. Every series takes about 400 seconds. Again, every second the sensor values are read out and the PID algorithm computes a new output value which is passed on to the current driver board.
The values of t_stable and ΔT are determined like before.
As it certainly takes longer to achieve lower temperatures, the time t_0 at which the setpoint temperature is reached for the first time and the difference

$$\Delta t = t_\mathrm{stable} - t_0 \tag{4.9}$$

is identified to make the measurements comparable. Furthermore the gap ΔT_over between the setpoint temperature and the maximum of the first overshoot is determined. The results are shown in table 4.6.
The first thing that should be noted is that the temperature stabilization is achieved for every setpoint temperature except one.

T_{set} / °C	ΔT / K	t_{stable} / s	Δt / s	t_0 / s	ΔT_{over} / K
27.62	1.22	170	165	52	2.50
25.12	3.60	94	82	12	2.82
22.62	6.16	71	52	19	2.57
20.12	8.58	94	68	26	2.38
17.62	10.83	93	69	24	2.13
15.12	13.17	116	84	32	1.94
12.62	15.77	112	67	45	1.63
10.12	18.28	138	74	64	1.32
7.62	20.86	145	66	79	0.94
5.12	23.42	162	56	106	0.63
2.62	26.11	205	51	154	0.25
0.12	28.61	–	–	–	–

Table 4.6: List of different gaps between setpoint and average room temperature and the respective stabilization times relative to the start of a measurement as well as to the time the setpoint temperature is reached first. Furthermore the depths of the first overshoots are given.

For setpoint temperatures between 2.62 °C and 25.12 °C the stabilization criterion is fulfilled roughly $50 - 80$ seconds after t_0. As an example, the temperature courses for the measurements with $T_{\text{set}} = 17.62\,°\text{C}$ and 2.62 °C are shown in figure 4.15.

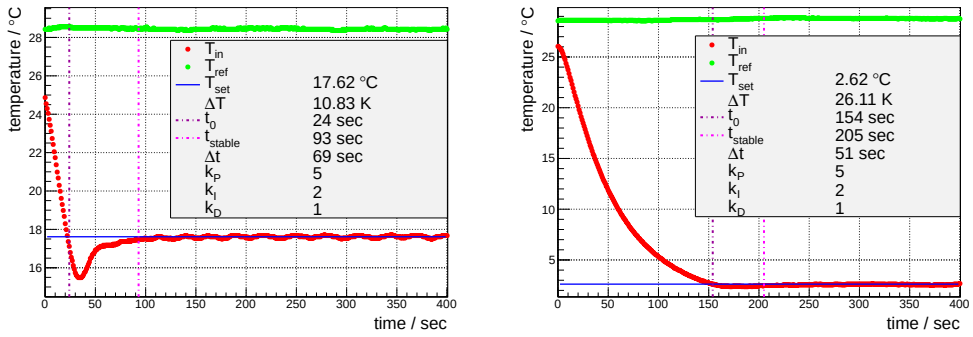

Figure 4.15: Temperature courses for the setpoint temperatures 17.62 °C (left) and 2.62 °C (right).

The main difference in the temperature courses is the depth of the first overshoot which gets smaller for lower setpoint temperatures. For $T_{\text{set}} = 27.62\,°\text{C}$ the over-

shoot's depth is 2.50 K and, therefore, more than twice as big as the difference between setpoint and room temperature (see fig. 4.16). Because of this it takes relatively long for the temperature to be stabilized, even though the setpoint temperature is reached only 5 seconds after starting the observation.
This could be because the Peltier element's cooling rates are high for small temperature differences between the cold and hot side and the set integral gain k_I prevents the controller from reacting fast enough to the rapid changes in the temperature's course.
Another reason for the large overshoot could be that the proportional gain k_P is too large for such high cooling rates and small gaps between T_in and the setpoint temperature. Further experiments with different parameter sets and high setpoint temperatures could reveal the exact cause, but are not necessary for this thesis since the temperature is still stabilized after approx. 3 minutes.

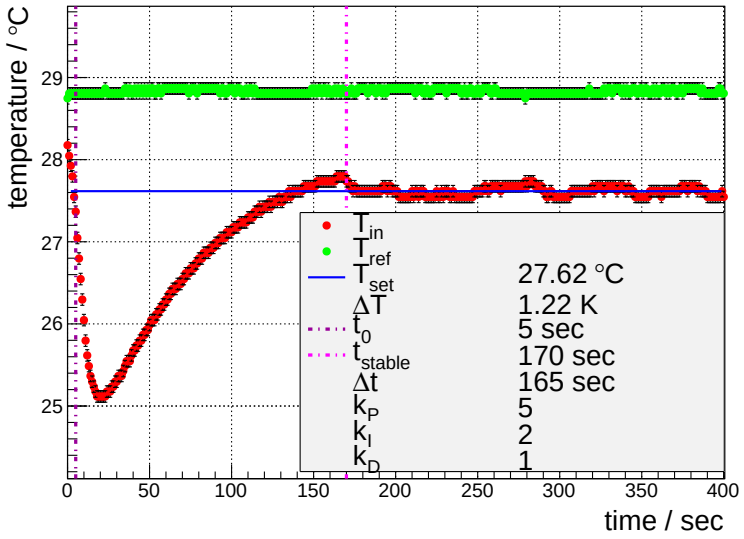

Figure 4.16: Temperature course for the setpoint temperature 27.62 °C.

For $T_\mathrm{set} = 0.12\,^\circ\mathrm{C}$ the stabilization criterion is not fulfilled during the measurement. This is not a failure of the parameter set for such low setpoint temperatures but due to the fact that the cooling system is at its limits here. As can be seen in fig. 4.17 the setpoint temperature cannot be reached. The lowest achievable temperature on the copper block's side opposite to the Peltier element is approx. 1 °C.
Besides this, the other measurements show that as long as the setpoint temperature lies inside the range of the cooling system, a stabilization for this temperature

can be reached within a few minutes ($t_{\text{stable}} = 205\,\text{s}$ for $T_{\text{set}} = 2.62\,°\text{C}$) without adjusting the control parameters.

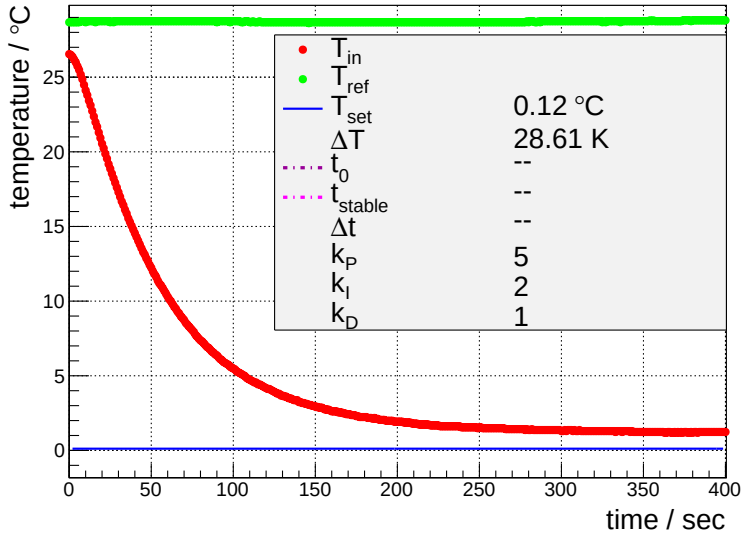

Figure 4.17: Temperature course for the setpoint temperature 0.12 °C.

5 Conclusion and Outlook

In the course of this bachelor's thesis a temperature stabilization system for silicon photomultipliers was developed using a Peltier-element-based cooling system, a programmable current source, and a PID controller.
The designed current driver board proved to work well providing 16 different direct current settings between 0 A and approximately 5 A with a step size of roughly 300 mA between two settings. Each of the settings can be set by the used microcontroller.
The examination of the cooling system consisting of a Peltier element with a mounted combination of a passive cooling element and a fan has shown that fast cooling rates up to $-2.40\,\frac{\mathrm{K}}{\mathrm{s}}$ can be achieved enabling the system to reach low temperatures within a couple of seconds. When the Peltier element is powered with the driver board's highest current setting, the lowest achievable temperature on the cold side is $-8.00\,^{\circ}\mathrm{C}$ at an ambient temperature of approx. $27\,^{\circ}\mathrm{C}$. Therefore the setup's range of reachable temperatures is well suited for working with SiPMs. The performance test also showed that the system that dissipates the heat from the Peltier element's hot side can be used in the full range of the current driver board. Even though it must be said that it comes to its limits for high electrical powers on the Peltier element.
Furthermore, the PID algorithm was successfully adjusted to the setup by finding a well working set of control parameters through comparison of different parameter combinations. Temperature stabilization was achieved and maintained over several minutes with a maximal deviation between setpoint and measured temperature of $\pm 0.14\,\mathrm{K}$.
Changing the setpoint temperature of the controller showed that the parameter set works well for all temperatures reachable by the cooling system. The time it takes until the temperature is stabilized depends on the difference between ambient temperature and setpoint temperature and is usually on the order of one minute after the setpoint temperature has been reached for the first time. Even for the lowest reachable temperatures it does not take much longer than three and a half minutes to cool down the copper block and stabilize the temperature.
The developed system works for setpoints from room temperature down to about $0\,^{\circ}\mathrm{C}$.

The setup can now be used as the basis for various temperature stabilization systems for SiPMs and is already part of experiments conducted in the course

of a master's thesis to be published [21]. But since every experimental setup is different, the adjustment of the control parameters has to be done according to purpose and structure of the given setup.
In some experiments it might not be possible to attach the Peltier element as close to the SiPM as in this case. So a larger volume of copper is needed to transfer the heat. Therefore, lower temperatures on the Peltier element's cold side have to be reached to obtain the same temperature at the front. This requires a better heat dissipation system for the Peltier element's hot side. Other options are to use more than one Peltier element or more powerful ones which would require a new current driver board, too.
A useful extension to the system could be a humidity sensor that may be used to prevent the SiPM's temperature from dropping below dew point so that no condensed water interferes with the measurements or even destroys the devices.
Regarding the behaivor of the controller for setpoints close to the ambient temperature, further experiments with different parameter settings could be conducted to make out the cause of the large first overshoot. According to the results of those measurements the program running on the microcontroller could be changed so it adjusts the PID algorithm to these circumstances to achieve an even faster temperature stabilization.
Another way to decrease the stabilization time could be to design a driver board that can also change the direction of the current so that the copper block can be actively heated as well when the temperature drops too far below the setpoint for example during the first overshoot. The heating could also be used when the SiPM's properties need to be studied at temperatures above room temperature.

A Appendix A

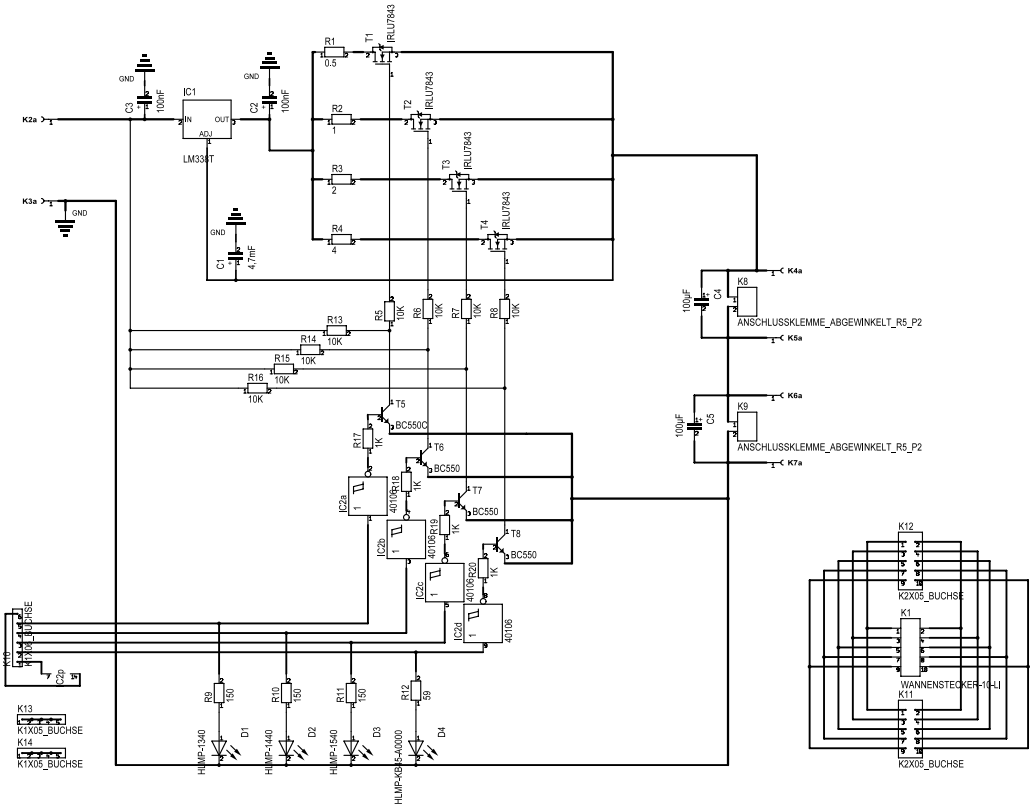

Figure A.1: Circuit diagram of the driver board "PeltierPapa v1.0".

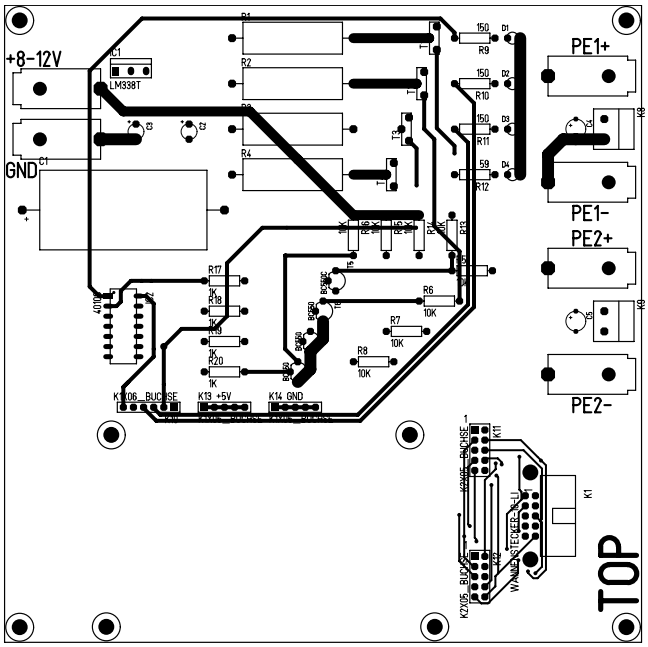

Figure A.2: Peltier current driver board design (top view).

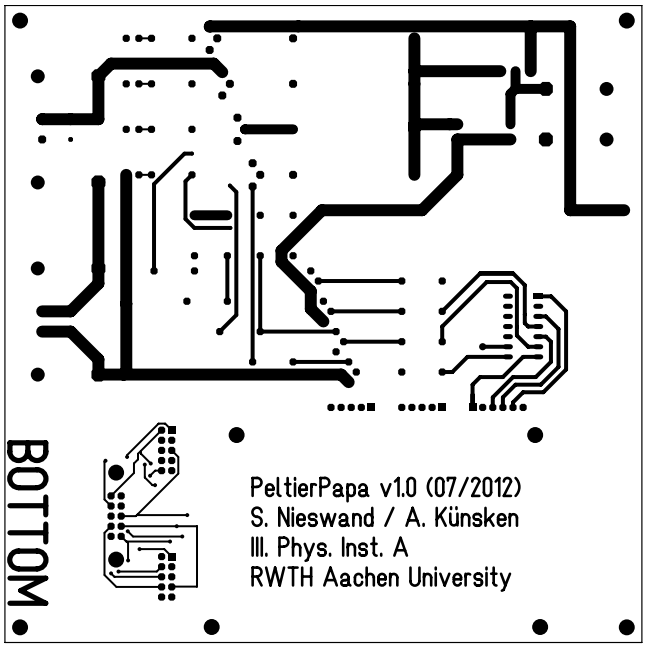

Figure A.3: Peltier current driver board design (bottom view).

Bibliography

[1] Hamamatsu Photonics. *MPPC Technical Information.* Available online http://sales.hamamatsu.com/assets/pdf/parts_S/high_resolution_mppc_kapd0002e08.pdf, visited 01.10.2012.

[2] Samuel Espana et al. *Performance Evaluation of SiPM Detectors for PET Imaging in the Presence of Magnetic Fields.* IEEE Nuclear Science Symposium Conference Record, pages 3591–3595, 2008.

[3] Jörg Rennefeld. *Studien zur Eignung von Silizium Photomultipliern für den Einsatz im erweiterten CMS Detektor am SLHC*, diploma thesis, III. Phys. Inst. B, RWTH Aachen University, 2010.

[4] Markus Lauscher. *Characterisation Studies of Silicon Photomultipliers for the Detection of Fluorescence Light from Extensive Air Showers*, master's thesis, III. Phys. Inst. A, RWTH Aachen University, 2012.

[5] Johannes Schumacher. *Characterization Studies of Silicon Photomultipliers: Noise and Relative Photon Detection Efficiency*, bachelor's thesis, III. Phys. Inst. A, RWTH Aachen University, 2011.

[6] Dieter Meschede. *Gerthsen Pysik.* Springer-Verlag Berlin Heidelberg, 24. edition, 2010.

[7] Yu. G. Gurevich, G. N. Logvinov, O. Yu. Titov, J. Giraldo. *New physical principles of contact thermoelectric cooling.* Surface Review and Letters, 9:1703–1708, 2002.

[8] Robert C. Weast et al. *Handbook of Chemistry and Phyisics. A Ready-Reference Book of Chemical and Physical Data.* CRC Press, 1st student edition, 1988.

[9] Gerhard Lutz. *Semiconductor Radiation Detectors.* Springer-Verlag Berlin Heidelberg, 2nd printing of 1st edition, 2007.

[10] J. Nagao, E. Hatta, K. Mukasa. *Evaluation of metal-*Bi_2Te_3 *contacts by electron tunneling spectroscopy.* 15th International Conference on Thermoelectrics, pages 404–407, 1996.

[11] J. Grehn and J. Krause. *Metzler Physik.* Schroedel, 4th edition, 2011.

[12] Simon M. Sze and Kwok K. Ng. *Physics of Semiconductor Devices*. Wiley, 2007.

[13] D. L. Greenaway, G. Harbeke. *Band structure of bismuth telluride, bismuth selenide and their respective alloys*. Journal of Physics and Chemistry of Solids, 26:1585–1604, 1965.

[14] Tellurex. *Frequently Asked Questions About Our Cooling And Heating Technology*. Available online http://www.tellurex.com/pdf/peltier-faq.pdf, visited 01.10.2012.

[15] Wolfgang Schneider. *Praktische Regelungstechnik*. Vieweg+Teubner Wiesbaden, 3. edition, 2008.

[16] Wikipedia article. *PID controller*. http://en.wikipedia.org/wiki/PID_controller, visited 01.10.2012.

[17] QuickCool. *Specifiation Sheet: Peltier element*. Available online http://www.produktinfo.conrad.com/datenblaetter/175000-199999/189180-da-01-en-PELTIER_ELEMENT_QC_31_1_4_8_5M.pdf, visited 01.10.2012.

[18] Fischer Elektronik. *Specifiation Sheet: Cooling element*. Available online http://www.farnell.com/datasheets/17561.pdf, visited 01.10.2012.

[19] SEPA. *Specifiation Sheet: MFB50E05 (Axial fan)*. Available online http://www.produktinfo.conrad.com/datenblaetter/175000-199999/189487-da-01-de-AXIALLUEFTER_50X50X10MM_5VDC_KUGELLAGER.pdf, visited 01.10.2012.

[20] Dallas Semiconductor. *Specifiation Sheet: DS18B20 (Programmable Resolution 1-Wire Digital Thermometer)*. Available online http://www.rentron.com/Files/ds18b20.pdf, visited 01.10.2012.

[21] Andreas Künsken. *Simulations of SiPMs and Validation via Measurements*, master's thesis to be published, III. Phys. Inst. A, RWTH Aachen University, 2012.

[22] National Semiconductor. *Specifiation Sheet: LM338T (5-Amp Adjustable Regulator)*. Available online http://www.farnell.com/datasheets/1640753.pdf, visited 01.10.2012.

[23] ON Semiconductor. *Specifiation Sheet: BC550C (Transistor)*. Available online http://www.farnell.com/datasheets/727135.pdf, visited 01.10.2012.

[24] International Rectifier. *Specifiation Sheet: IRLU7843 (MOSFET)*. Available online http://www.irf.com/product-info/datasheets/data/irlr7843pbf.pdf, visited 01.10.2012.

[25] Philips Semiconductors. *Specifiation Sheet: HEF40106B (Schmitt trigger)*. Available online http://www.powersystems.com.uy/robotica/archivos/40106.pdf, visited 01.10.2012.

[26] Hameg Instruments. *Specifiation Sheet: HMP4040 (Programmable Power Supply)*. Available online http://www.rapidonline.com/pdf/85-4424.pdf, visited 01.10.2012.

[27] Fluke. *Manual: 8845A (Digital Multimeter)*. Available online http://174.123.170.1/admincp/files/manuals/Fluke-8846A.pdf, visited 01.10.2012.

[28] Arduino Webpage. http://arduino.cc/en/Main/ArduinoBoardMega2560, visited 01.10.2012.

Acknowledgements - Danksagung

Hiermit möchte ich mich bei allen Leuten bedanken, die mir das Erstellen dieser Arbeit ermöglicht haben. Da ich hier nicht alle helfenden Personen namentlich aufführen kann, sei an dieser Stelle mein Dank gegenüber denjenigen Leuten ausgedrückt, die hier nicht erwähnt werden.
Besonderer Dank geht an Herrn Prof. Dr. Hebbeker, dafür, dass er mir die Möglichkeit gegeben hat, meine Bachelorarbeit an seinem Institut anzufertigen.
Des Weiteren bedanke ich mich bei meinem Betreuer Herrn Dr. Markus Merschmeyer, der mir von Anfang an sowohl bei der Entwicklung und Duchführung der Experimente, als auch beim Schreiben der Arbeit jederzeit hilfreich zur Seite stand und auch bei mehrmaligem Erklären eines Sachverhalts nie die Geduld verlor.
Weiterhin geht mein Dank an Andreas Künsken, mit dem ich im Rahmen seiner Masterarbeit eng zusammengearbeitet habe und der stets für jegliche Fragen offen war und mir vorallem beim Schreiben der Microcrontroller-Software und der Auswertung der gewonnenen Daten per ROOT geholfen hat.
Bedanken möchte ich mich auch bei allen Mitarbeitern der CMS-Arbeitsgruppe, die immer bereit waren, Fragestellungen zu den verschiedensten Themen zu diskutieren. Diese Personen einschließend geht mein Dank auch an alle anderen Büropartner und -nachbarn, die mir die Zeit am Institut durch ihre offene und freundliche Art sehr angenehm gestaltet haben und die immer für sinnvolle und manchmal auch für weniger sinnvolle Gespräche zur Verfügung standen.
Repräsentativ für die Mitarbeiter der elektronischen und der mechanischen Werkstatt, möchte ich mich bei Herrn Zantis, Herrn Adamczyk und bei Herrn Philipps bedanken, ohne deren Hilfe und Beratung die Realisierung des Versuchsaufbaus nicht möglich gewesen wäre.
Für das Korrekturlesen meiner Arbeit danke ich noch einmal Herrn Dr. Markus Merschmeyer und Andreas Künsken und weiterhin Florian Scheuch und Felix Lensing.
Abschließend bedanke ich mich bei meiner Familie und meinen Freunden für die mentale Unterstützung während der sehr lehrreichen und interessanten aber manchmal auch sehr stressige Zeit der letzten Monate.

Erklärung

Hiermit versichere ich, dass ich diese Arbeit einschließlich beigefügter Darstellungen und Tabellen selbstständig angfertigt und keine anderen als die angegebenen Hilfsmittel und Quellen verwendet habe. Alle Stellen, die dem Wortlaut oder dem Sinn nach anderen Werken entnommen sind, habe ich in jedem Fall unter genauer Angabe der Quellen deutlich als Entlehnung kenntlich gemacht.
Aachen, Oktober 2012

Simon Nieswand